Journal of Oceanology and Limnology
Vol. 38 No. 4, P. 1018-1044, 2020
**https://doi.org/10.1007/s00343-020-0110-x**

# Research progress of $TiO_2$ photocathodic protection to metals in marine environment*

WANG Xiutong[1, 2, 3, 4, **], XU Hui[1, 2, 3], NAN Youbo[1, 2, 3], SUN Xin[1, 2, 3], DUAN Jizhou[1, 2, 4], HUANG Yanliang[1, 2, 4], HOU Baorong[1, 2, 4]

[1] *Key Laboratory of Marine Environmental Corrosion and Bio-fouling, Institute of Oceanology, Chinese Academy of Sciences, Qingdao 266071, China*

[2] *Open Studio for Marine Corrosion and Protection, Pilot National Laboratory for Marine Science and Technology, Qingdao 266237, China*

[3] *University of Chinese Academy of Sciences, Beijing 100049, China*

[4] *Center for Ocean Mega-Science, Chinese Academy of Sciences, Qingdao 266071, China*

Received Mar. 3, 2020; accepted in principle Apr. 2, 2020; accepted for publication Apr. 30, 2020


**Abstract** Corrosion protection has become an important issue as the amount of infrastructure construction in marine environment increased. Photocathodic protection is a promising method to reduce the corrosion of metals, and titanium dioxide ($TiO_2$) is the most widely used photoanode. This review summarizes the progress in $TiO_2$ photogenerated protection in recent years. Different types of semiconductors, including sulfides, metals, metal oxides, polymers, and other materials, are used to design and modify $TiO_2$. The strategy to dramatically improve the efficiency of photoactivity is proposed, and the mechanism is investigated in detail. Characterization methods are also introduced, including morphology testing, light absorption, photoelectrochemistry, and protected metal observation. This review aims to provide a comprehensive overview of $TiO_2$ development and guide photocathodic protection.

**Keyword**: photocathodic protection; corrosion; titanium dioxide ($TiO_2$); photoelectrochemistry; metal

## 1 INTRODUCTION

As need for the marine economy increases, an increasing number of structures, including offshore platforms, marine pipelines, and marine wharfs, have been built with large quantities of steel and other metals. Steel has been the most popular construction material because of its low cost, high strength and good machinability. In marine environments, the corrosion of steel is very severe because of the presence of oxygen, sunshine, microorganisms, $Cl^-$ and other ions.

In a survey project led by Hou from the Institute of Oceanology, Chinese Academy of Sciences (IOCAS), it was found that the cost of corrosion in China was approximately 310 billion USD in 2014, equivalent to 3.34% of the GDP (Hou et al., 2017; Hou, 2019). In the shipbuilding industry, approximately 9% of income is spent on corrosion protection and repair. However, many factors can play roles in the corrosion of metals in seawater, such as temperature, dissolved oxygen, salinity, and microorganisms, which cause deterioration and failure of metal materials with long exposure times (Melchers, 2003). Among these factors, the effect of $Cl^-$ is especially remarkable; even metals with high corrosion-resistance performance, such as stainless steel, can be affected by the high concentration of $Cl^-$, which induces pitting-type corrosion (Tsutsumi et al., 2006, 2007).

To reduce the corrosion of metals in marine environments, many methods have been proposed, such as coating, corrosion inhibitors and cathodic protection (CP). Among these methods, CP has been widely used for metals with high efficiency, and it has

* Supported by the CAS Strategic Priority Project (No. XDA13040404), the National Natural Science Foundation of China for Exploring Key Scientific Instrument (No. 41827805), and the Shandong Key Laboratory of Corrosion Science
** Corresponding author: wangxiutong@qdio.ac.cn

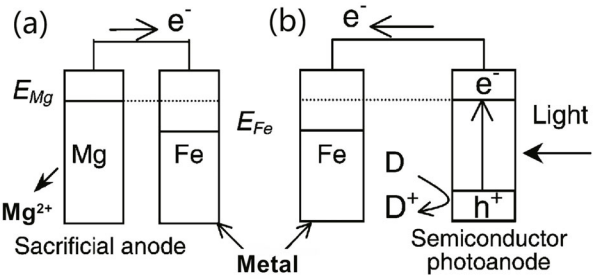


**Fig.1 Scheme and electron transfer of sacrificial anode cathodic protection (SACP) (a) and photocathodic protection (b)**

Reprinted with permission (Park et al., 2001). Copyright 2001, Royal Society of Chemistry.

a long research history of almost 200 years since its first application in the protection of copper ship sheeting (Davy, 1824).

Corrosion is a process in which electrons flow from the metal, and CP technology is a method to decrease the metal potential; thus, redox reactions on metal surfaces are inhibited, and the corrosion rate is reduced. For traditional CP, two main methods have been designed for the marine industry. The first is sacrificial anode cathodic protection (SACP), which uses an active metal with a negative corrosion potential such as magnesium, zinc and aluminum to provide electrons, and the anodes are consumed during the protection. The second method is impressed current CP (ICCP), which uses a rectifier or potentiostat as an external power source to provide current to keep the metal in the proper potential range. For an SACP system, the quantity of sacrificial anodes depends on the dimensions and service life of the structure; however, the production of the anodes requires a considerable amount of energy consumption, and the anodes dissolve in seawater and thus cause pollution and harm to the marine ecology. For the ICCP system, stable power supplies and complicated maintenance devices are needed, which would be difficult in some offshore conditions, and large amounts of energy are also necessary during the duty life of the structure.

In recent years, photocathodic protection has been proposed as a new type of technology that utilizes green and sustainable solar energy to provide the current to protect metals from corrosion. A semiconductor can utilize light and produce electrons that are transferred to the metal to reduce the corrosion rate. Photocathodic protection is similar to sacrificial anode CP (Park et al., 2001), and the mechanism is illustrated in Fig.1.

Yuan and Tsujikawa (1995) investigated the photoeffect of $TiO_2$ coatings on copper substrates under ultraviolet illumination for the first time. In the last three decades, a considerable amount of effort has been devoted to photocathodic protection for metals by using many types of semiconductors, such as $TiO_2$, $SrTiO_3$, g-$C_3N_4$, $In_2O_3$ and ZnO (Yuan et al., 1994; Huang et al., 2000; Ohko et al., 2001; Liu et al., 2007; Bu et al., 2011, 2013; Li et al., 2014, 2015b; Sun et al., 2014, 2015; Zhang et al., 2015a; Yang and Cheng, 2018). Among these materials, $TiO_2$ is the most widely used material and serves as a photoanode due to its low cost, high stability, nontoxicity and easy availability.

Since Fujishima and Honda (1972) established a method of water photolysis in which $TiO_2$ is subjected to light irradiation, the photocatalytic performance of $TiO_2$ and other semiconductors has been investigated in many fields, such as wastewater treatment (Nagaveni et al., 2004), sterilization (Matsunaga et al., 1988), dye-sensitized solar cells (O'Regan and Grätzel, 1991), self-cleaning (Wang et al., 1998; Balaur et al., 2005), and biomedical fields (Oh et al., 2005). When the energy of the irradiation light is higher than the bandgap (Eg), there are three steps in the photocatalysis: first, the electrons and holes separate, where the electrons are excited from the valence band (VB) to the conduction band (CB) and the holes remain in the VB; second, the excited carriers, including electrons and holes, migrate to the surface; third, the carriers react with electron donors (D) and electron acceptors (A) (Guo et al., 2019). This process is shown in Fig.2. The carrier transmission process under light irradiation includes the generation and transportation of electrons and holes.

However, $TiO_2$, with a relatively wide bandgap (approximately 3.2 eV), can absorb only ultraviolet light, which makes up approximately 5% of sunlight. On the other hand, during migration, recombination occurs on the surface and in the bulk. These two drawbacks have limited the applications of $TiO_2$ in photocatalysis and energy harvesting (Cai et al., 2019).

There are three types of $TiO_2$ often used in photoelectrochemistry: rutile, anatase, and brookite. Different $TiO_2$ types can affect the charge transfer and bandgap levels and rutile and anatase are most widely used. Many methods have been used to increase the visible light response and reduce the recombination of $TiO_2$, such as energy band engineering, morphology

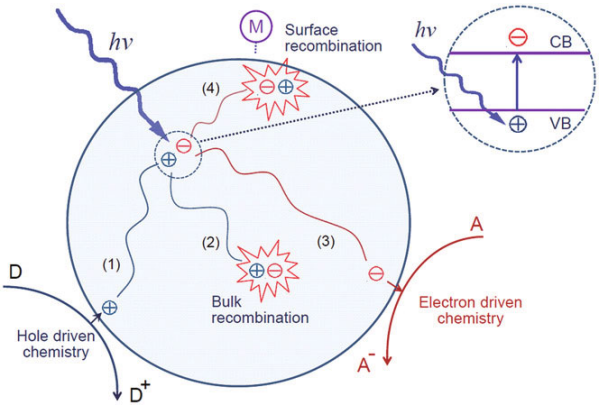


**Fig.2 Schematic diagram of excitation transfer processes in photocatalysis**

Reprinted with permission (Guo et al., 2019). Copyright 2019, American Chemical Society.

control, nanoassembly, electronic structure calculations and molecular dynamics simulations (Linsebigler et al., 1995; Tong et al., 2012). Among these methods, material doping is the most commonly used, and it includes metal doping, such as V, Cr, Mn, Fe and Ni (Paramasivam et al., 2012); nonmetal doping, such as N, C, S, B, P and F (Fujishima et al., 2008); metal oxide doping, such as niobates, tantalates, vanadates and germanates (Tong et al., 2012); and narrow bandgap semiconductor coupling (Chen et al., 2012). In addition to the strong catalytic property and high charge mobility, cost and stability are also important parameters of the new type of material for the photoanode (Kudo and Miseki, 2009).

Structures with different dimensionalities (0D, 1D, 2D, 3D) and different energy facets (001, 101) can exhibit special properties (Li and Wu, 2015), as proposed in Fig.3. The appropriate nanostructure has high solar energy conversion and results in better photocatalytic activities. Nanoparticles, as 0D structures, usually have a large surface area and are used as photocatalysts in the suspended state, and the small particle size can increase the number of active sites. 1D structures such as nanotubes, nanobelts and nanowires mostly have large length-diameter ratios, which can enhance charge transport along the longitudinal direction. 2D nanomaterials such as nanosheets and films can reduce the distance between photoexcited carriers and increase photon absorption due to the large area. 3D nanostructures can adopt unique arrangements using precise and self-assembly strategies, and specific performance can be obtained.

However, in addition to the dimensions of the nanostructure, the facet design is also important; three-dimensional hierarchical spheres of anatase $TiO_2$ with exposed $TiO_2$ (001) facets and single-crystal nanosheets have superior photoactivity (Yang et al., 2009; Chen et al., 2010), as illustrated in Fig.4.

In this review, we summarize the recent progress in the application of $TiO_2$ in the field of photocathodic protection. The modification and mechanism are discussed, and characterization and analysis techniques are also introduced.

## 2 $TiO_2$ MODIFICATION AND APPLICATION

$TiO_2$ tends to be modified by semiconductors in the following three ways: increasing the separation efficiency of photogenerated electron-hole pairs, decreasing the conduction band potential of the semiconductor and changing the redox potential of the electrolyte. A sufficiently negative CB potential is required for photoelectrochemical CP. Hitherto, based on these strategies, researchers have synthesized $TiO_2$ nanotube photoanodes and modified them by increasing the surface area, doping, sensitizing quantum dots, and combining different semiconductors to extend their functionalities in the visible range. Coupling with narrow-bandgap semiconductors, metals and nonmetals are used for photocathodic protection, and the protected metal tends to be polarized into a safe range under visible light (Li et al., 2017a; Bu et al., 2018).

### 2.1 $TiO_2$ preparation

There are several methods to synthesize $TiO_2$, such as the hydrothermal process, the sol-gel method, liquid phase deposition, and anodization. During the hydrothermal process of $TiO_2$, pH, and temperature are the key factors determining morphology, and different materials lead to distinct properties. Liu et al. (2018) employed a $TiCl_4$ solution as the Ti source with a pH of 5–6 at 180°C and obtained $TiO_2$ nanoparticles. Zhang et al. (2010) selected titanium foil with a porous $TiO_2$ film as the source of Ti to obtain a three-dimensional $TiO_2$ NT network under hydrothermal conditions, and the structure could be useful in photocatalysis and other fields. Lan et al. (2018) assembled a uniform and ordered $TiO_2$ nanosheet by the hydrothermal-induced solvent-confined method, and the assembly is illustrated in Fig.5.

Through the sol-gel method, $TiO_2$ film can be synthesized by aging of a $TiO_2$ sol liquid, coating this liquid on the metal surface and then heating. Shen et al. (2005) used tetra-n-butyl titanate and ethyl

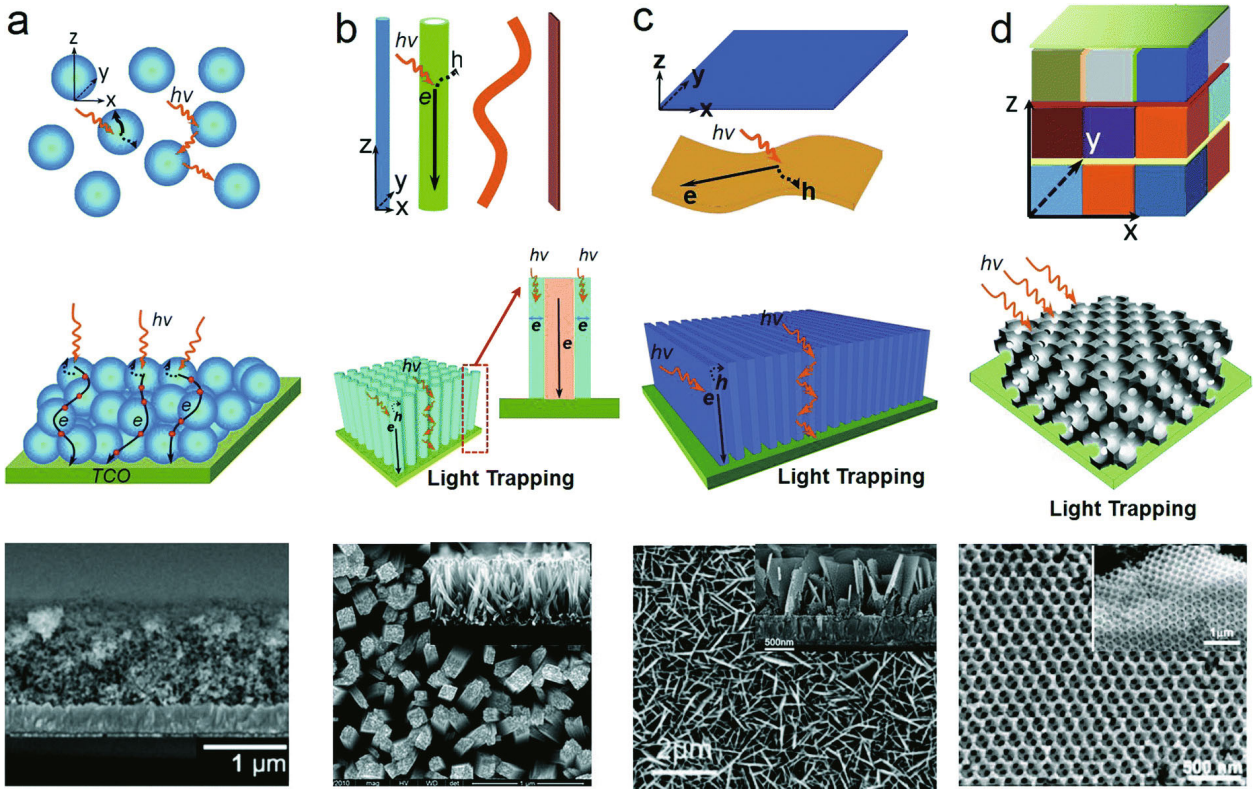


**Fig.3 SEM images of light trapping and structuring with different dimensions**

a. 0D nanoparticles; b. 1D nanorods; c. 2D nanosheets; d. 3D porous crystal-constructed photoelectrodes. Reprinted with permission (Li and Wu, 2015). Copyright 2015, Royal Society of Chemistry.

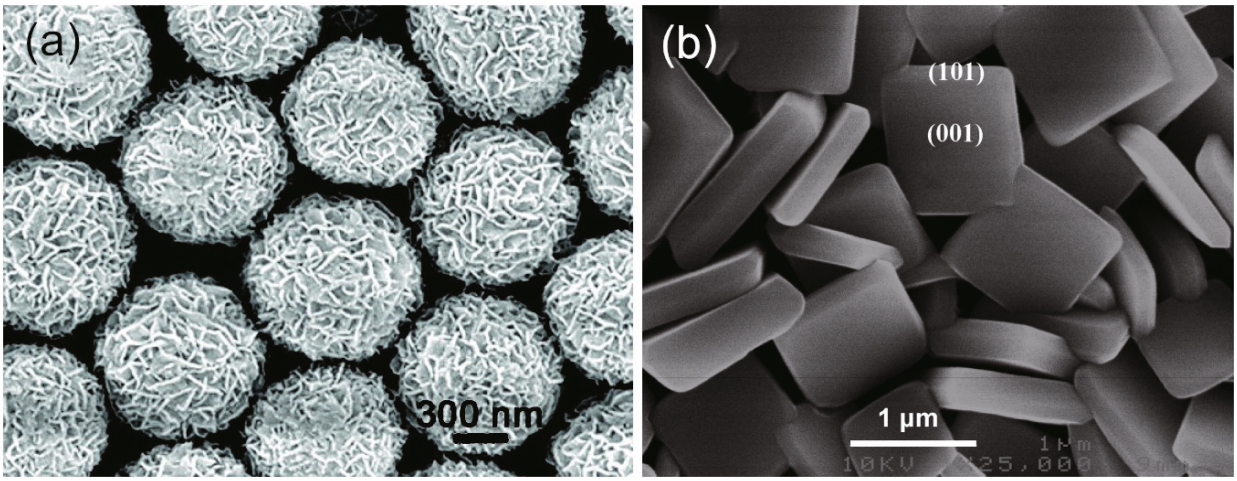


**Fig.4 Anatase $TiO_2$ spheres (a) and single-crystal nanosheets with an exposed $TiO_2$ (001) facet (b)**

a. reprinted with permission (Chen et al., 2010). Copyright 2010, American Chemical Society; b. reprinted with permission (Yang et al., 2009). Copyright 2009, American Chemical Society.

acetoacetate as raw materials to synthesize a $TiO_2$ sol and then distributed the sol on the steel substrate using the dip-coating method. The coatings showed good corrosion resistance. In the sol-gel method, it is easy to control the coating thickness; however, the films usually crack during heating. To avoid this, Shen et al. (2005) soaked the $TiO_2$ film in boiling water for 10 min, and the cracks decreased with less heating time. Zhu et al. (2010) also developed a combined sol-gel and hydrothermal method and prepared a 3D titanium nanowire network. Liquid-phase deposition is a useful method in which a $TiO_2$ film can be prepared on an ITO substrate surface, and the substrate is placed vertically at a low temperature

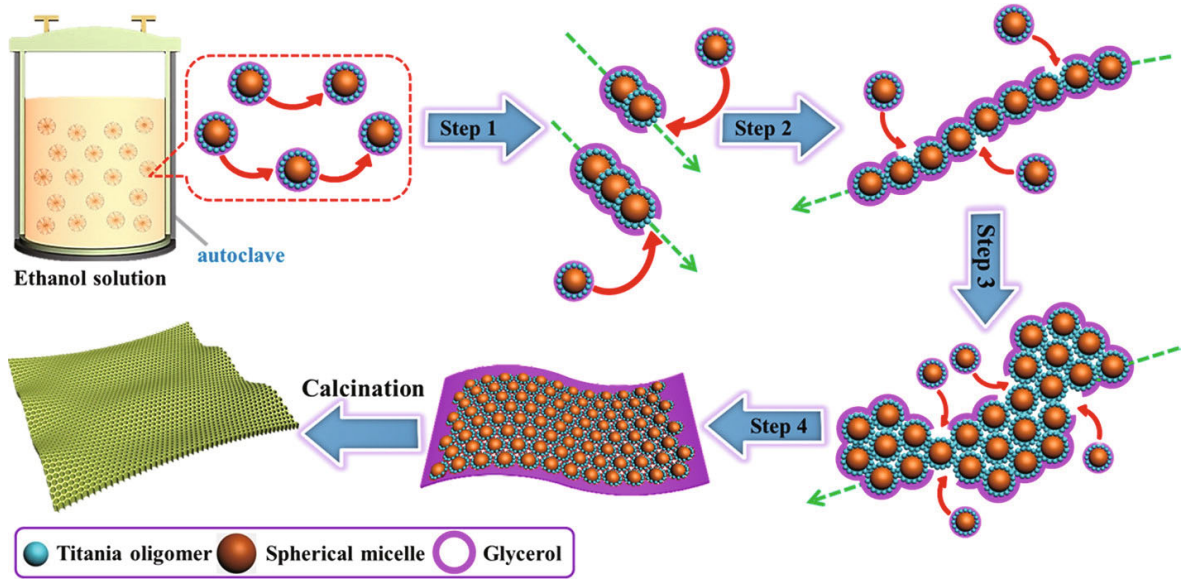


**Fig.5 Schematic illustration of the fabrication of $TiO_2$ nanosheets via the hydrothermal method**

Reprinted with permission (Lan et al., 2018). Copyright 2018, American Chemical Society.

(less than 100°C). Lei et al. (2012) used $(NH_4)_2TiF_6$ and $H_3BO_3$ as precursor bath solutions. After drying naturally and annealing in air, $TiO_2$ is obtained.

Anodization is an effective method to prepare nanotubes, and it has been widely used in the preparation of $TiO_2$. In general, titanium foil materials need to be cleaned in polishing solutions containing acetone, ethanol, and deionized water. During anodization, titanium foil and platinum sheets are connected to the positive and negative poles of the DC power supply, respectively. The structure of the nanotubes depends on the electrolyte, temperature, potential, etc. Recently, two-step anodization has been proposed and applied, including two processes with different applied powers and times. The first step is to obtain a glossy surface that could provide a better growth environment for the nanotubes in the next anodization step. Finally, annealing is used to increase the crystallinity, and the time and temperature can vary based on the proportion of rutile and anatase $TiO_2$ (Roy et al., 2011).

### 2.2 Sulfide modified $TiO_2$

As mentioned above, modification is the most widely used method to improve the photocatalytic performance of $TiO_2$, and many materials are used to modify and dope $TiO_2$. Among these materials, sulfide compounds are very popular because of their superior performance.

CdS is a type II-VI semiconductor with a bandgap of 2.4 eV, and its photoelectron transmission capacity is preeminent. Li et al. (2011) coated CdS nanoparticles onto $TiO_2$ nanotube arrays, and the composite could protect the metals under UV and visible light. However, CdS is sensitive to photocorrosion, and Boonserm et al. (2017) investigated the reaction during the measurement and found that corrosion of the nanocomposite film decreased the photocurrent. However, it is difficult to simultaneously achieve both high electron transmission efficiency and superior redox capacity.

ZnS has some properties similar to those of CdS, such as nontoxicity and chemically stable performance. It has been reported that a ZnS coating can protect CdS and CdTe from photocorrosion (Lin et al., 2010; Zhang et al., 2015a). Construction of Z-scheme photocatalytic systems consisting of two semiconductors as photoexcitation systems, with the constructor located at the interface to reduce the contact resistance, is increasing in popularity. Zhu et al. (2019) employed CdS to modify $TiO_2$ nanowires, prepared a ZnS shell to protect CdS from photocorrosion and added Ag as an electron transporter between CdS and $TiO_2$. Upon coupling with the composite, the potential of 403SS decreased to -1 174 mV (vs. SCE), and the photocurrent reached 19.97 mA/cm$^2$. The absorption edge was nearly 700 nm, and the visible absorption range increased because the energy of the incident ray was absorbed by the noble metal. Moreover, surface plasmon resonance might be triggered. CdTe (Eg=1.47 eV) is an ideal photoelectric conversion material that has a

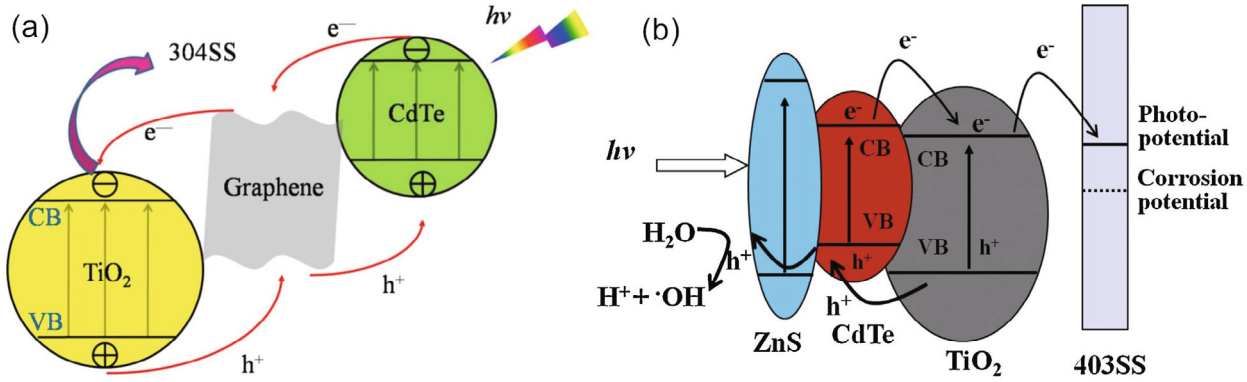


**Fig.6 Mechanism of CdTe/GR/$TiO_2$ (a) and ZnS/CdTe/$TiO_2$ (b) composite for corrosion protection**

a. reprinted with permission (Li et al., 2015a). Copyright 2015, IOP Publishing; b. reprinted with permission (Zhang et al., 2015a). Copyright 2015, Elsevier.

very high optical absorption coefficient (>104/cm) and good overlap with the solar spectrum (Li et al., 2015a). The light absorption range of the CdTe/$TiO_2$ composite film can be expanded to the visible region by adjusting the size of the quantum dots, which can capture electrons and generate multiple electron-hole pairs ($e^-$-$h^+$) under illumination. The photoelectric conversion efficiency was very high after CdTe quantum dots were used to modify $TiO_2$. However, the stability of CdTe is the main problem hindering practical application. To improve the stability of CdTe QDs, ZnS shells were deposited on CdTe/$TiO_2$ composite films. The results showed that the ZnS/CdTe/$TiO_2$ composite film had excellent photoelectrochemical properties (Zhang et al., 2015a), and the mechanism is illustrated in Fig.6.

$Sb_2S_3$ is also used to modify $TiO_2$ because of its narrow bandgap. Some experiments have been performed, and the results show that the bandgaps of $Sb_2S_3$/$Sb_2O_3$/$TiO_2$ and $Sb_2O_3$/$TiO_2$ are approximately 2.02 eV and 3.32 eV, respectively, revealing that $Sb_2S_3$ reduces the bandgap. It is also known that $Sb_2S_3$ is a p-type semiconductor, and when it combines with an n-type semiconductor, for example, $TiO_2$ and $Sb_2O_3$, the Fermi level of different materials flattens; at the same time, a built-in electric field forms, which can drive electron transfer (Li et al., 2018b). Similarly, the bandgap of $Ni_3S_2$ is 2.5 eV, making this material also appropriate to modify $TiO_2$. Nan et al. (2019) found that the photocurrent increased to 53.1 μA/$cm^2$, which is higher than that of pure $TiO_2$. In a double electrolytic cell working with a three-electrode system coupled with $Ni_3S_2$, the potential of 304SS decreased to a minimum of -720 mV (vs. SCE) with 0.1 mol/L $Na_2S$ and 0.2 mol/L NaOH as the hole scavenger solution and 3.5 wt.% NaCl as the corrosive solution, simulating a marine environment. Compared with $TiO_2$, the composite has stronger absorption in the visible region. In addition, the UV-Vis spectroscopy showed that the absorption is redshifted, indicating that the forbidden band energy decreases; the mechanism is shown in Fig.7.

The direct bandgap of SnS is approximately 1.4 eV, and the optical absorption coefficient $\alpha$ is larger than $10^4$/cm. SnS is nontoxic, inexpensive and environmentally compatible. Sn is one of the most promising materials because of its good photoconductivity and nonlinear optical response. SnS has been proven to have good photocatalytic performance in the application of photocatalysis. It has been reported that SnS can be used as a sensitizer of $TiO_2$. Therefore, it is of great significance to apply SnS/$TiO_2$ composites to photocathode protection (Shao et al., 2018).

The CB of $Ag_2S$ (0.3 eV) is higher than that of $TiO_2$ (0.1 eV), and the VB of $Ag_2S$ (0.7 eV) is lower than that of $TiO_2$ (3.1 eV). Therefore, nontoxic $Ag_2S$ cosensitized with $TiO_2$ can improve the separation of photogenerated electron-hole pairs and accelerate the transfer of carriers. The $Ag_2S$/$TiO_2$ composite has higher visible light utilization than pure $TiO_2$. Under visible light, the photochemical properties of the $Ag_2S$/$TiO_2$ composite are better than those of pure $TiO_2$, so the composite can be used to protect stainless steel (Ning et al., 2017; Yang et al., 2019). $Bi_2S_3$ is an attractive material due to its narrow bandgap (Eg=1.3 eV) and high photoelectric conversion efficiency. It can absorb almost all visible light from the solar spectrum. There is a strong interface electron field between $Bi_2S_3$ nanoparticles and $TiO_2$ nanotube arrays. The electric field increases the separation of photogenerated carriers and then reinforces the photoelectrochemical properties (Hu et al., 2017; Li

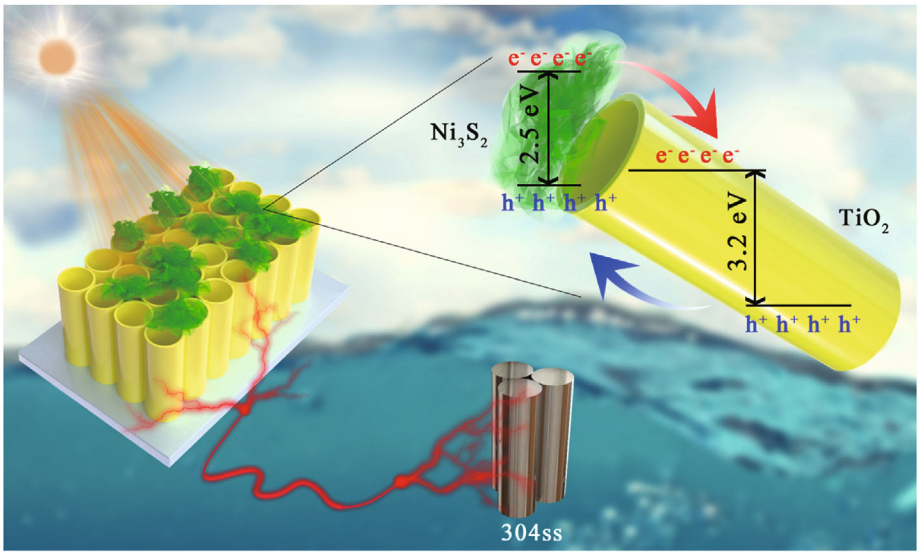


**Fig.7 Mechanism of $Ni_3S_2/TiO_2$ photocathodic protection for 304SS**

Reprinted with permission (Nan et al., 2019). Copyright 2019, Elsevier.

et al., 2017a; Guan et al., 2018b). The narrow bandgap doping mechanism is shown in Fig.8 (Li et al., 2017a; Yang et al., 2019). MnS has excellent photoelectric performance and is mainly used as a buffer material, photoelectric device and magnetic component of many important diluted magnetic semiconductors. Although MnS has a wide bandgap (3.7 eV), as a p-type semiconductor, it can form a p-n heterojunction with $TiO_2$ (n-type semiconductor). The inherent field in the p-n heterojunction can reduce the recombination of photogenerated electrons and holes, which is beneficial to the photoelectric properties of materials (Ge et al., 2015).

$ZnIn_2S_4$ is a ternary sulfur compound with a narrow bandgap of 2.34–2.48 eV, which is significantly narrower than that of $TiO_2$. It is widely used as a visible light-responsive photocatalyst. In addition, the potential at the bottom of the CB of $ZnIn_2S_4$ is -0.74 eV, and the potential at the top of VB is more positive than the oxygen-producing potential. Therefore, $ZnIn_2S_4$ is a promising photoanode material in photoelectrochemistry. As an n-type semiconductor, it can form a heterojunction electric field at the interface when it is combined with $TiO_2$. It is obvious that $ZnIn_2S_4$ can promote the separation of electrons and holes, and the $TiO_2/ZnIn_2S_4$ composite has enhanced charge transfer and photocatalytic degradation properties (Li et al., 2018a, 2019). $AgInS_2$ is a nontoxic and environmentally friendly visible photosensitizer, and it is an ideal photoelectric conversion material to replace toxic cadmium sulfide. It has potential for application in the field of photoelectrochemical conversion and photocatalysis. The bandgap of $AgInS_2$ is between 1.87 and 2.03 eV, and the CB and VB of $AgInS_2$ are 1.08 eV and 0.83 eV, respectively, with unique absorption in the visible and near-infrared regions. Sensitization of the ordered $TiO_2$ NTs by $AgInS_2$ QDs can significantly improve the PEC conversion efficiency in the visible region, and the ternary structure of $AgIn_xS_y$-sensitized $TiO_2$ also enhances visible light photocatalytic activity (Sun et al., 2018a).

Selenide and telluride are similar to sulfide, as Se and Te belong to the VIA family, and these compounds manifest semiconductor properties and have already been applied in the field of photoelectrochemistry. For example, ZnSe has attracted great interest due to its small bandgap (2.7 eV) and outstanding photoelectric properties (Zhang et al., 2015b). $NiSe_2$-doped $TiO_2$ NTs broaden the response range of visible light, and CdSe has a bandgap of 1.6–1.8 eV and can thus absorb visible light (Li et al., 2015b; Wang et al., 2016a). It has been reported that $Bi_2Se_3$ is an ideal n-type semiconductor with a bandgap of 0.35 eV, and it is a distinctive topological insulator with a conductive surface and dielectric body structure. Hence, the absorption coefficient of $Bi_2Se_3$ is high in the visible and near-infrared regions (Wang et al., 2018a). CdTe is also used in the protection of metals, and Wang (Yang et al., 2016b) coated CdTe on $TiO_2$ nanotubes using the potentiodynamic deposition method. The potential of stainless steel upon coupling decreased to -850 mV (vs. SCE), and the composite promoted the absorption of visible light.

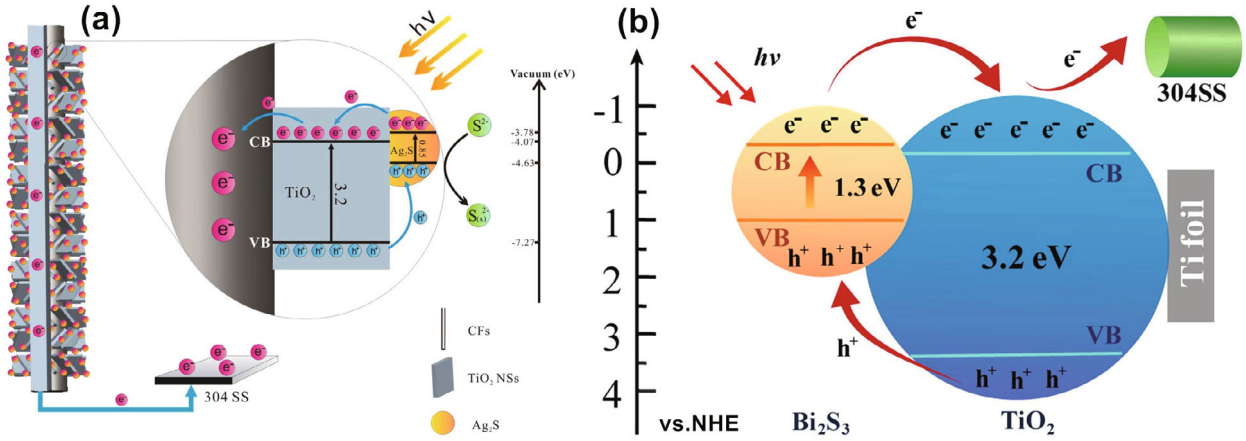


**Fig.8 Schematic illustration of $Ag_2S$ QDs sensitized CFs-$TiO_2$ (a) and $Bi_2S_3$/$TiO_2$ doping (b)**

a. reprinted with permission (Yang et al., 2019). Copyright 2019, Elsevier. b. reprinted with permission (Li et al., 2017a).

### 2.3 Metal-doped $TiO_2$ material

To improve the photoelectrochemical response, Au, Ag and Ni were doped into $TiO_2$ to prepare wide-light-response composite materials. However, the doping of noble metals may introduce additional defects into the lattice structure of the $TiO_2$ substrate, increase the recombination rate of photogenerated carriers, and lead to the loss of photoelectrochemical activity. Therefore, an appropriate element content needs to be maintained.

Ag is one of the most important noble metals used to decorate $TiO_2$ nanotubes. The surface plasmon resonance (SPR) effect of Ag nanoparticles on $TiO_2$ can prolong the visible light response and improve the absorption capacity of $TiO_2$. SPR occurs when the oscillation frequency of the incident electromagnetic field matches that of the free electron under visible light (Ma et al., 2020). The energy of the incident ray is absorbed, and the absorption of visible light extends due to the proper distribution of the Ag nanoparticles (Guan et al., 2019), as shown in Fig.9. In addition, the high Schottky barrier between Ag nanoparticles and $TiO_2$ materials can prevent the recombination of photogenerated electrons and holes, thus promoting the electron transfer process. Therefore, the combination of Ag nanoparticles on $TiO_2$ NTs is a promising way to improve the corrosion protection performance of 304SS under visible light (Li et al., 2014). Another noble metal, Au, is also exploited in the same field. There have been some reports about Au and $TiO_2$ composites. Zhu et al. (2013) proposed that the Au/$TiO_2$ compound with ZnS could prevent electrons from flowing from the substrate/Au surface into the Au/solution owing to the potential barrier, as the conduction band (1.85 eV vs. NHE) is higher than the Fermi level of Ag (+0.5 eV vs. NHE).

Research on Fe doping has been carried out as well; iron can enter the lattice of $TiO_2$, thus destroying the integrity of $TiO_2$ and generating defect dots, which plays an important role in provoking the separation of photoelectrons and holes in promoting photocatalytic activity (Li et al., 2007). It has been found that iron ions can improve the photocatalytic activity of $TiO_2$, and $TiO_2$ doped with iron can be used as an energy storage agent, which can maintain corrosion resistance for a long time in the dark (Liu et al., 2014; Momeni et al., 2018).

When Ni is substituted for Ti atoms, oxygen vacancies are produced in $TiO_2$, which promote the transfer of photoinduced electrons, improve the photoelectric conversion efficiency of $TiO_2$ under visible light, and improve the corrosion resistance. Sun et al. (2013) found that Ni doping introduced an impurity energy level that was higher than the $TiO_2$ valence band, thus decreasing the conduction band, which hence remained negative. Therefore, Ni-doped $TiO_2$ has a visible light response, and Ni doping is conducive to the photoelectrochemical corrosion resistance. With the increase in the Ni doping amount, the main doping mode is gap doping. However, the content of oxygen vacancies decreases during this process. Excessive Ni will form recombination centers of electrons and holes in $TiO_2$, which will worsen the visible light response performance.

Vanadium is an inhibitor used in paint. Thus, Chen et al. (2019) prepared V-doped $TiO_2$ through a sol-gel solution. In the composite, V atoms entered the $TiO_2$ lattice, which enhanced the anti-corrosion capability. Cerium nitrate is also a corrosion inhibitor applied in aqueous corrosive media. Li et al. (2012) exploited cerium nitrate to synthesize a Ce-doped $TiO_2$ film.

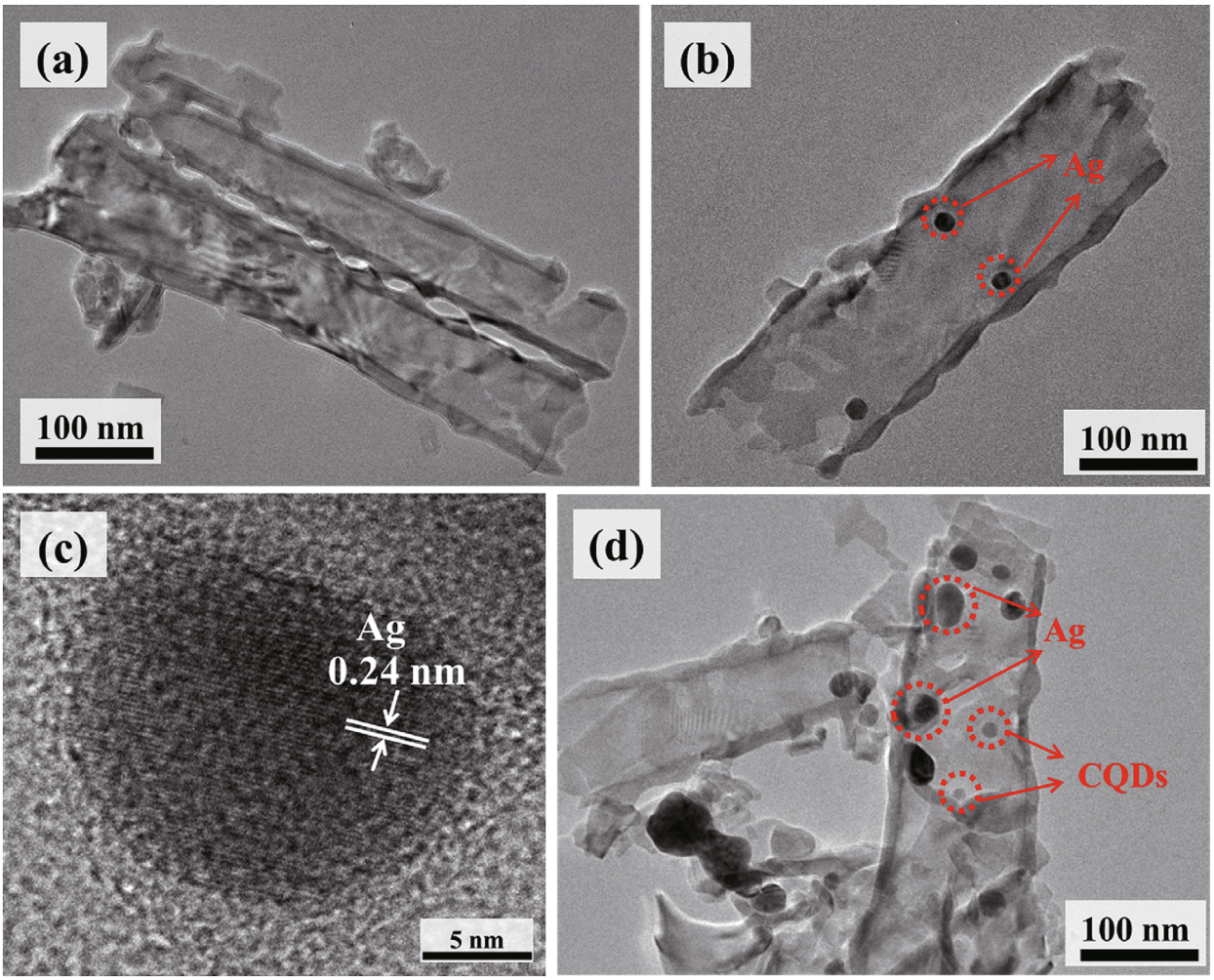


**Fig.9 TEM images of the $TiO_2$ (a), low (b) and high (c) magnifications of $Ag/TiO_2$, and $CQDs/Ag/TiO_2$ composite (d)**

Reprinted with permission (Guan et al., 2019). Copyright 2019, Elsevier.

Due to the suppression of $Ti^{4+}$, the transfer capacity of photogenerated electron-hole pairs increased, and recombination decreased. The absorption edge of the composite thus redshifted. However, metal doping increased the efficiency of electron transfer to the protected metal, and the mechanism is shown in Fig.10.

### 2.4 Metal-oxides/$TiO_2$

Metal-oxides usually have unique structures and appropriate bandgaps to enhance the light absorption of $TiO_2$ to achieve high photocatalytic performance.

ZnO has a photovoltaic effect and a bandgap similar to that of $TiO_2$, and the electron mobility in zinc oxide is approximately three times that of $TiO_2$. High electron mobility can effectively reduce the secondary recombination of photoinduced electron-hole pairs, thus significantly improving the lifetime of the carriers. Therefore, ZnO has a higher photoelectric conversion potential, and the potential of ZnO is more negative than that of $TiO_2$. Xu et al. (2014) designed a $ZnO/TiO_2$ composite using a simple hybrid sol-gel-powder method (Xu et al., 2014). The OCP of 304SS coupled with the $ZnO/TiO_2$ film was up to -730 mV (vs. SCE) in 3 wt.% NaCl at an annealing temperature of 500°C, and the absorption of the composite film redshifted. Multilayered $ZnO/TiO_2$ coatings exhibited anticorrosion performance on 304SS (Boukerche et al., 2019). However, ZnO has a wide energy gap of 3.37 eV, which still needs to be ameliorated in the synthesis and structure.

As an n-type semiconductor, $\alpha$-$Fe_2O_3$ has been verified to absorb almost 40% of the solar spectrum, but $\alpha$-$Fe_2O_3$ also has a short carrier diffusion length, high electron hole binding rate and poor electron mobility (Xue et al., 2020). Cui and Pei (2019) prepared $TiO_2$ nanotubes modified with $Fe_2O_3$ particles. Theoretically, the bandgap of the $Fe_2O_3$/

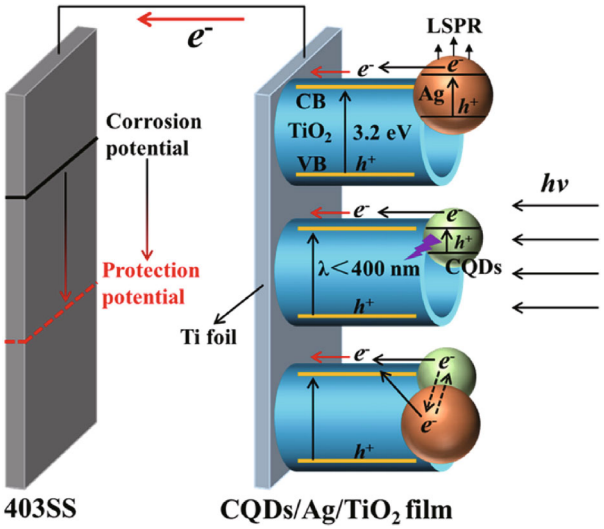


**Fig.10 Schematic mechanism of the CQDs/Ag/$TiO_2$ composite film as a photoanode for photocathodic protection**

Reprinted with permission (Guan et al., 2019). Copyright 2019, Elsevier.

$TiO_2$ composite is 2.2 eV; thus, it has a wider spectrum response than pure $TiO_2$. Furthermore, the photocurrents of pure $TiO_2$ and the $Fe_2O_3/TiO_2$ composite are 90 and 400 μA/cm$^2$, respectively. Therefore, nontoxic Fe has good performance in photocathode protection (Deng et al., 2015). $V_2O_5$ can store electrons and cations, and $TiO_2/V_2O_5$ composite materials can serve as photoelectrodes for light energy conversion and storage (Zhou et al., 2012).

The indirect bandgap energy of $In_2O_3$ is 2.8 eV, so $In_2O_3$ is an effective semiconductor material with a visible light response. $In_2O_3$ has a good band structure, with a CB bottom of -0.63 eV, a VB of +2.17 eV and a conduction band potential that is more negative than the corrosion potential of steel. Therefore, $In_2O_3$ is a potential anti-corrosion anode under visible light irradiation. In addition, there are many oxygen vacancies in $In_2O_3$ that can affect the photoelectrochemical conversion. Keeping the structure unchanged, oxygen vacancies can improve the photoelectric conversion performance and effectively expand the visible light absorption area (Sun and Chen, 2015).

$Bi_2O_3$ (p-type semiconductor) is the simplest Bi-based oxide. Due to its excellent properties, such as high dielectric constant, refractive index and photoluminescence, it has been widely used in a wide range of photoelectrochemical applications. There are six polymorphic forms of $Bi_2O_3$: α-$Bi_2O_3$, β-$Bi_2O_3$, γ-$Bi_2O_3$, δ-$Bi_2O_3$, ε-$Bi_2O_3$ and ω-$Bi_2O_3$ (triclinic). Among these polymorphs, β-$Bi_2O_3$ has a unique tetragonal crystal structure, resulting in a narrow bandgap (2.3–2.8 eV) and providing a transport channel for photogenerated electrons and holes. Therefore, β-$Bi_2O_3$ is a suitable candidate for $TiO_2$ nanotube modification. More importantly, if p-$Bi_2O_3$ and n-$TiO_2$ are integrated into composite materials, a p-n heterojunction will be formed at the interface, which can significantly improve the separation efficiency of photogenerated electrons and holes (Guan et al., 2018a). The slow discharging of 304SS and the potential variation of 403SS are shown in Fig.11. After light exposure, it can be seen that the potential of both 304SS coupled with $TiO_2/V_2O_5$ and 403SS coupled $TiO_2/Bi_2O_3$ composites increase slowly in the dark, and both values are lower than the original corrosion potential of metals.

### 2.5 Polymer and special structure design

Some inhibitors are now applied for photogenic CP, such as polypyrrole (PPy) and polyaniline (PANI), which are both types of conductive polymers. Conducting polymers are conductive and have conjugated sequences of double and single bonds, and they participate in corrosion protection by forming compact and protective oxide films on the surface of the substrate.

PANI has benzenoid and quinonoid units and has a good ability to transport holes into n-type semiconductors. PANI is one of the most attractive conductive polymer materials and is widely used in the field of photoelectrochemistry (Zhang et al., 2017b). PANI exhibits the properties of p-type semiconductors. Combining PANI with p-type $TiO_2$ increases the final photoelectric field. In addition, an appropriate amount of PPy is helpful for photosensitization, heterojunction formation and the electron pool effect. Under white light irradiation, PPy provides sufficient photocathodic protection to Q235 carbon steel. Many researchers have fabricated PPy on $TiO_2$ composites (Lenz et al., 2003; Cui et al., 2015; Ren et al., 2016) to form synergistic interactions and increase the protective properties relative to those of the individual materials. Moreover, the addition of $TiO_2$ nanoparticles altered the surface of PPy to introduce more sites of interaction with the corrosion product. Polyacrylate was also applied in $TiO_2$ coating through the liquid-phase deposition method at 80°C (Lei et al., 2013) and formed hierarchical superstructures due to the interaction between these materials. The composite showed a higher photocurrent and lower potential than the original

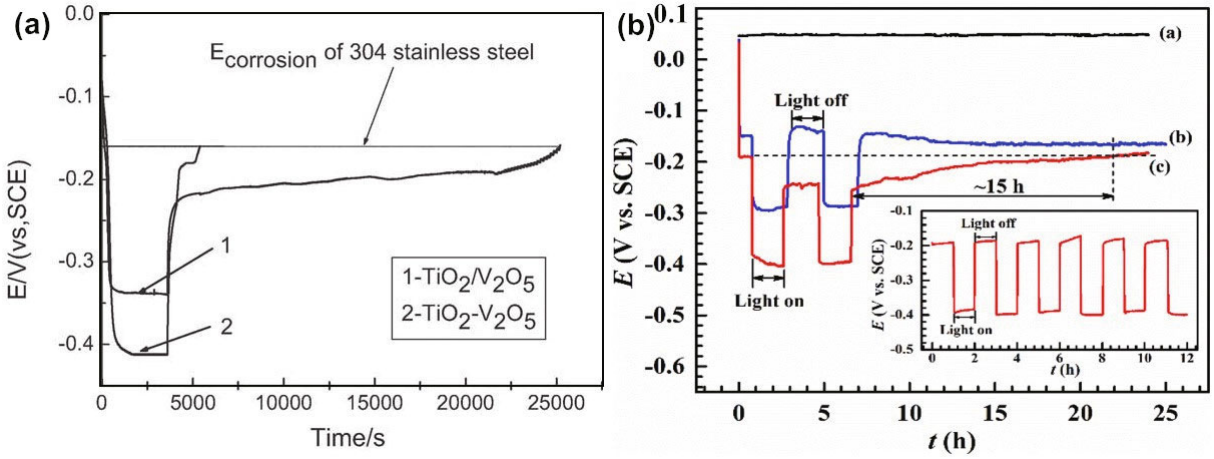


**Fig.11 Discharge progress of $TiO_2/V_2O_5$ composite coupling with 304SS (a) and potential variation of 403SS coupled with the β-$Bi_2O_3$-$TiO_2$ NTA film (b)**

a. reprinted with permission (Zhou et al., 2012). Copyright 2012, Wiley-VCH; b. reprinted with permission (Guan et al., 2018a). Copyright 2018, Elsevier.

material; thus, polyacrylate could offer photocathodic protection to the metal.

$SrTiO_3$ is a well-known solid semiconductor material with high photoelectric activity. The bandgaps of $SrTiO_3$ and $TiO_2$ are similar, approximately 3.2 eV, and $SrTiO_3$ is a p-type semiconductor with a perovskite structure. It was found that the $SrTiO_3/TiO_2$ composite could increase the charge separation rate and thus improve the photoelectrochemical properties (Zhu et al., 2014; Bu et al., 2018).

The structure of layered hydroxides (LDHs) consists of cation metal layers and interlayers of a charge-balanced anion. Researchers have been inspired, and some follow-up work is being executed. Based on zinc oxide, LDHs have a strong absorption rate of visible light. In iron-based LDHs, an oxygen bridge decreases the recombination of electron-hole pairs and extends the effective diffusion distance of the holes. In addition, after heat treatment, semiconductor properties are exhibited by ZnAlFe-LDH materials (Wang et al., 2018b). Therefore, LDHs are applicable to $TiO_2$ modification.

Crystalline tin dioxide ($SnO_2$) is an important n-type semiconductor. Its photoelectrochemical properties are similar to those of $TiO_2$, and the electron mobility of $SnO_2$ is higher than that of $TiO_2$ for single crystals and the corresponding nanostructures. The conduction band edge of $SnO_2$ is lower than that of $TiO_2$, so the conduction band of $SnO_2$ can be used as an electron pool to preserve electrons in the case of coupling of photogenerated electrons. Thus, the $SnO_2$ coating can be used as a kind of energy storage material, and the $SnO_2/TiO_2$ electrode has a good CP effect on 304SS in the dark (Subasri and Shinohara, 2003; Li et al., 2014; Hu et al., 2015a, b).

$Co(OH)_2/TiO_2$ has been reported to have improved electrochemical properties relative to pure $TiO_2$ because $Co(OH)_2$ has a good ability to capture photogenic holes and provide additional reaction sites. To accelerate the transfer velocity of electrons, the binary mixture requires other components; for example, Xie et al. (2018) and Lu et al. (2020) added graphene to the mixture.

The above modification is mainly focused on improving the photoelectric conversion efficiency, and there are some modifications that provide CP without light by introducing semiconductors with charge storage capacity into $TiO_2$ photoanodes, such as $WO_3$ (Guan et al., 2018b). $WO_3$ has a narrow bandgap of 2.6 eV and is responsive to visible light. In particular, due to the electrochemical reduction of $WO_3$, it has the ability to store energy, which makes it possible to protect metals in the dark. When $TiO_2$ is illuminated, electrons are excited from the VB to the CB. There are two pathways for electrons injection into the metal and acceptance by $WO_3$, which is reduced to consequently tungsten bronze ($M_xWO_3$, M=H, Li, Na, etc.; $x \leq 1$) and in this process, the electrons were stored (Tatsuma et al., 2001). Zhou et al. (2009) prepared a $TiO_2/WO_3$ bilayer coating that provided 6-h photocathodic protection after 1 h of irradiation. In addition to $WO_3/TiO_2$ coating, $WO_3$ can be deposited as nanoparticles on $TiO_2$ nanotube arrays, resulting in synergistic effects between 1D and 3D nanostructures (Sun et al., 2018b). Yu et al. (2018)

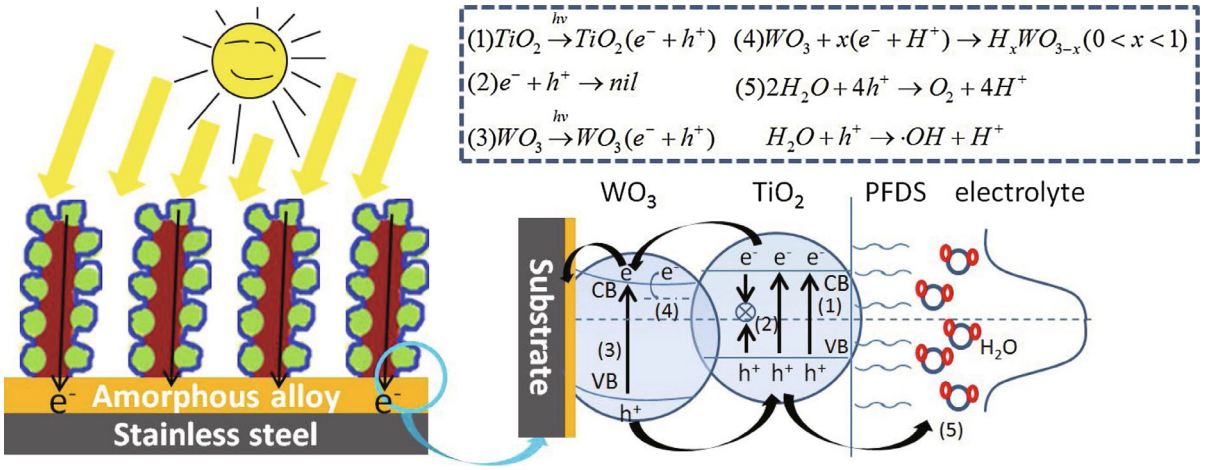


**Fig.12 Schematic diagram of the photocathodic protection of $WO_3$@$TiO_2$-coated 316 SS under illumination**

Reprinted with permission (Yu et al., 2018). Copyright 2018, Elsevier.

combined CP with superhydrophobicity by constructing $TiO_2$ nanoparticles and $WO_3$ nanosheet compounds. In the complex of a substrate with a $TiO_2$/$WO_3$ coating, Yu et al. (2018) found that some amorphous particles were present and were likely to prevent pitting corrosion. The antisepsis method prevents electron consumption; $WO_3$ can preserve electrons, and the mechanism is discussed. Therefore, $WO_3$ is considered to be a good way to modify $TiO_2$ (Jing et al., 2016), and the process is illustrated in Fig.12.

$CeO_2$ has widespread application in organic-dye-free solar cells, and it has been reported that the bandgap of $CeO_2$ is shifted by 80 nm compared to that of $TiO_2$. Some researchers have started to employ it in photocathodic protection. Subasri et al. (2006) found that the $CeO_2$/$TiO_2$ bilayer coating had better photocathodic protection than the coating of $CeO_2$ alone, although $CeO_2$ had better conductivity. For the bilayer coating, the outer $TiO_2$ coating accepts light to generate photoelectrons, and photoelectrons spread to the substrate across $CeO_2$. Subasri et al. (2006) also found that the protection of Cu lasted for 40 h after the light was turned off.

Zuo et al. (2018) prepared three kinds of nanotubes with different morphologies and used a schematic diagram to simulate and depict the behavior of incident light and reflected light. The flower-like nanostructure has the most voids where light has more probability to reflect and scatter. For the nanorod structure, the regular array and straight-pipe structure have less obstruction to stop incident rays escaping from the surface. Thus, with sufficient voids, flower-like $TiO_2$ showed the best photocathodic protection, highest photocurrent, lowest potential and smallest charge transfer resistance. Li et al. (2010) also prepared a flower-like N-$TiO_2$ film with a two-level nanostructure and found that the composite showed good CP even in the dark. The different nanostructures with LDHs, nanoflowers, spheres, and N-doped flower-like doping for $TiO_2$ are illustrated in Fig.13.

Special methods such as hydrogenation and UV radiation strategies are also used to modify the $TiO_2$ nanostructure. Wei et al. (2016) tried to improve the photoelectrochemical properties via hydrogenated $TiO_2$ nanotubes (H-$TiO_2$). After hydrogenation, the surface structure of H-$TiO_2$ was disordered, and oxygen vacancies and $Ti^{3+}$ were introduced. As a result, the photocurrent density was 1.20 mA/cm$^2$ at 0.7 V under simulated light. Zhang et al. (2017a) irradiated the surface of a $TiO_2$ nanotube array film with UV light. In subsequent photoelectric tests, the photocurrent increased by 50% compared with that of pristine $TiO_2$, and the corrosive potential negatively shifted to -678 mV (vs. SCE) in 3.5 wt.% NaCl and 0.01 mol/L NaOH. The reason for this phenomenon is that UV treatment contributed to the formation of hydroxyl groups on the $TiO_2$ surface, and the presence of hydroxyl groups accelerated the recombination of photogenerated electrons and holes descend and the water oxidation reaction. The open circuit potential variation of 304SS coupled with $TiO_2$ film with the treatment of hydrogenation and UV irradiation is shown in Fig.14.

## 3 CHARACTERIZATION OF $TiO_2$ PHOTOCATHODIC PROTECTION

The photocathodic protection performance of $TiO_2$ and semiconductor-doped composites on metal surfaces is the most important concern for researchers.

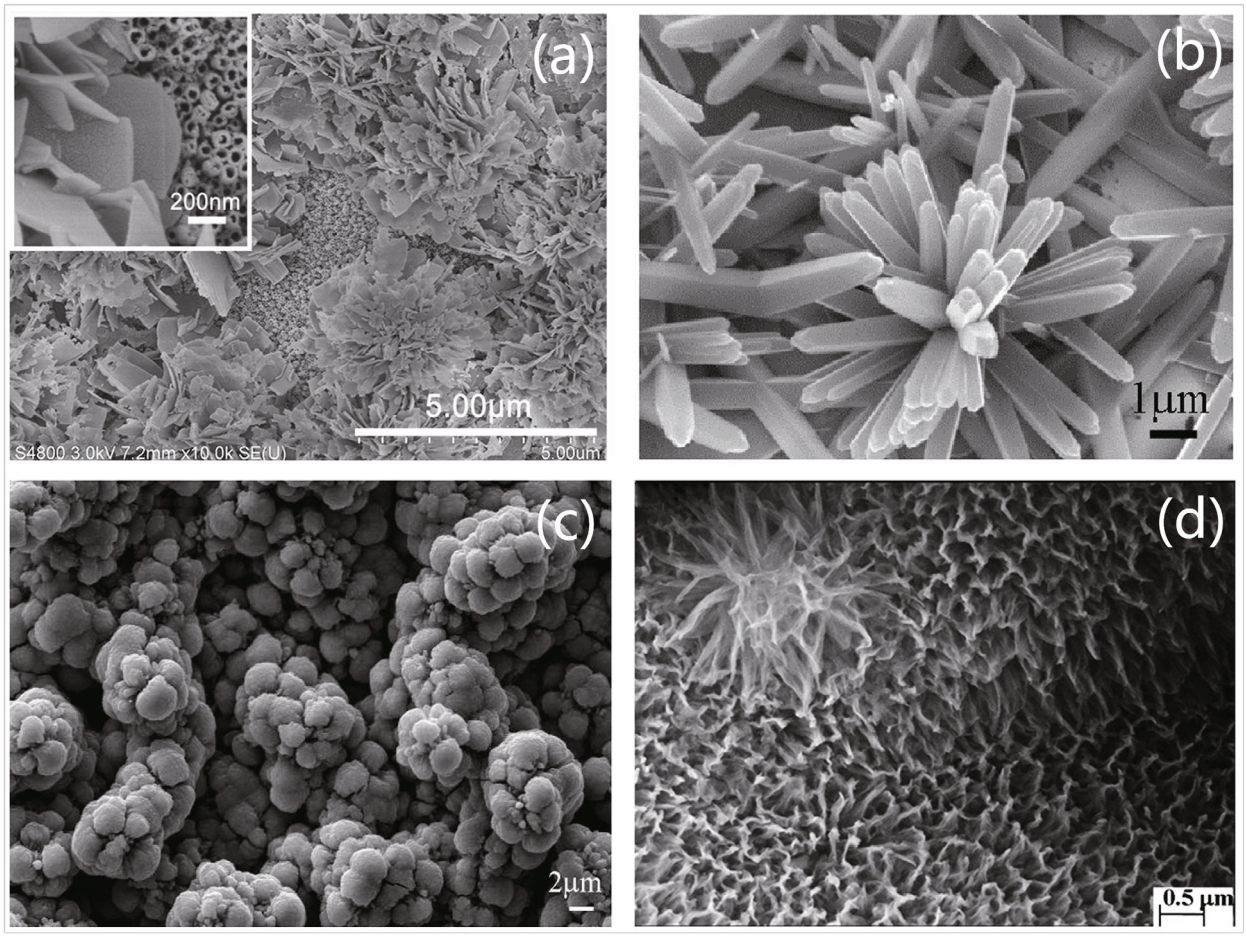


**Fig.13 Nanostructure with LDHs (a), nanoflower (b), sphere-like (c), N-doped flower-like doping with $TiO_2$ (d)**

a. reprinted with permission (Wang et al., 2018b); b & c. reprinted with permission (Zuo et al., 2018). Copyright 2018, Elsevier; d. reprinted with permission (Li et al., 2010). Copyright 2010, Elsevier.

Characterization of the materials not only focuses on the physical and chemical properties, such as photocatalytic properties, but also includes the protection effect for metals under different conditions, such as the protection potential of a metal during long-term continuous activity.

### 3.1 Morphology and structure characterization

Observing the morphology is usually the first step when investigating the surface of $TiO_2$ nanocomposites. The structure is an important factor that determines the properties of materials doped with $TiO_2$. From scanning electron microscopy (SEM) images, some characteristics can be known, such as the thickness of the surface film, the size of the nanoparticles and nanotubes, and the interspace of clusters (Lenz et al., 2003). In Fig.15, carbon fibers (CFs) as substrates and $TiO_2$ nanosheets with the (001) facet can be seen clearly in the FESEM images (Yang et al., 2019).

Transmission electron microscopy (TEM) can also be used to observe the surface morphologies of the surface films. Specifically, the crystallization of the microcrystal plane and the lattice fringe spacing can be determined from the TEM images. In addition, TEM, including high-resolution TEM (HRTEM) and selected-area electron diffraction (SAED), can distinguish the internal structure of crystals and growth direction, and it has a higher definition than SEM. From the TEM and HRTEM images in Fig.16, the distribution of $ZnIn_2S_4$ nanosheets on the $TiO_2$ nanotube structure is very clear, as are the lattice spacing and the corresponding facet (Li et al., 2019).

X-ray diffraction (XRD) is a technology that satisfies Prague's law to confirm whether $TiO_2$ is crystalline or amorphous, determine the specific phase structure qualitatively, and utilize the crystallization direction to verify the element composition (Yuan and Tsujikawa 1995; Ma et al., 2020). Ding et al. (2019) confirmed through XRD that $TiO_2$ was an amorphous phase and caused no obvious essential change in the g-$C_3N_4$ spectrum except for increasing the peak intensity and shifting the peaks to

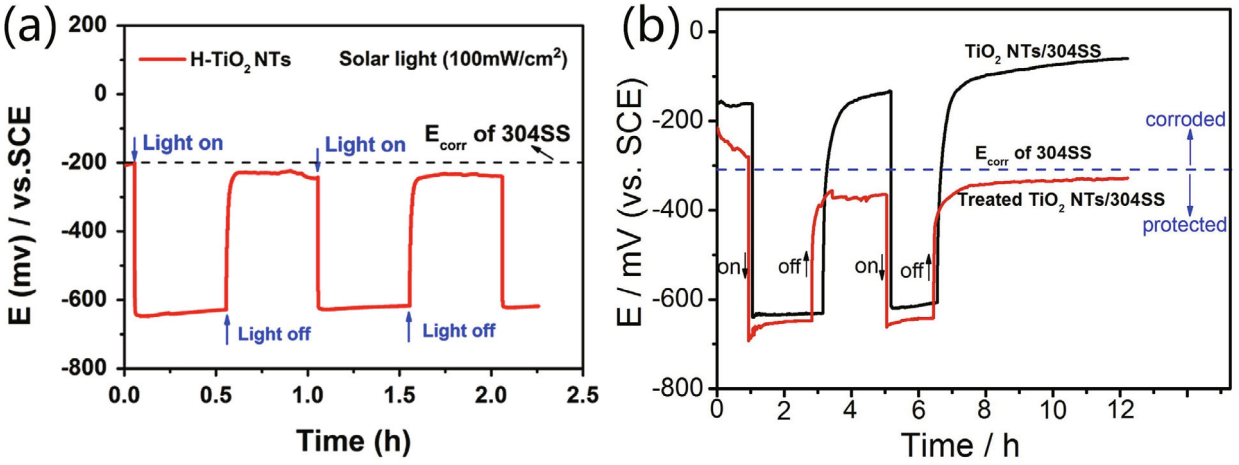


**Fig.14 OCP of 304SS connected with hydrogenation (a) and UV-treated $TiO_2$ NTs (b)**

a. reprinted with permission (Wei et al., 2016). Copyright 2016, Elsevier; b. reprinted with permission (Zhang et al., 2017a). Copyright 2017, Elsevier.

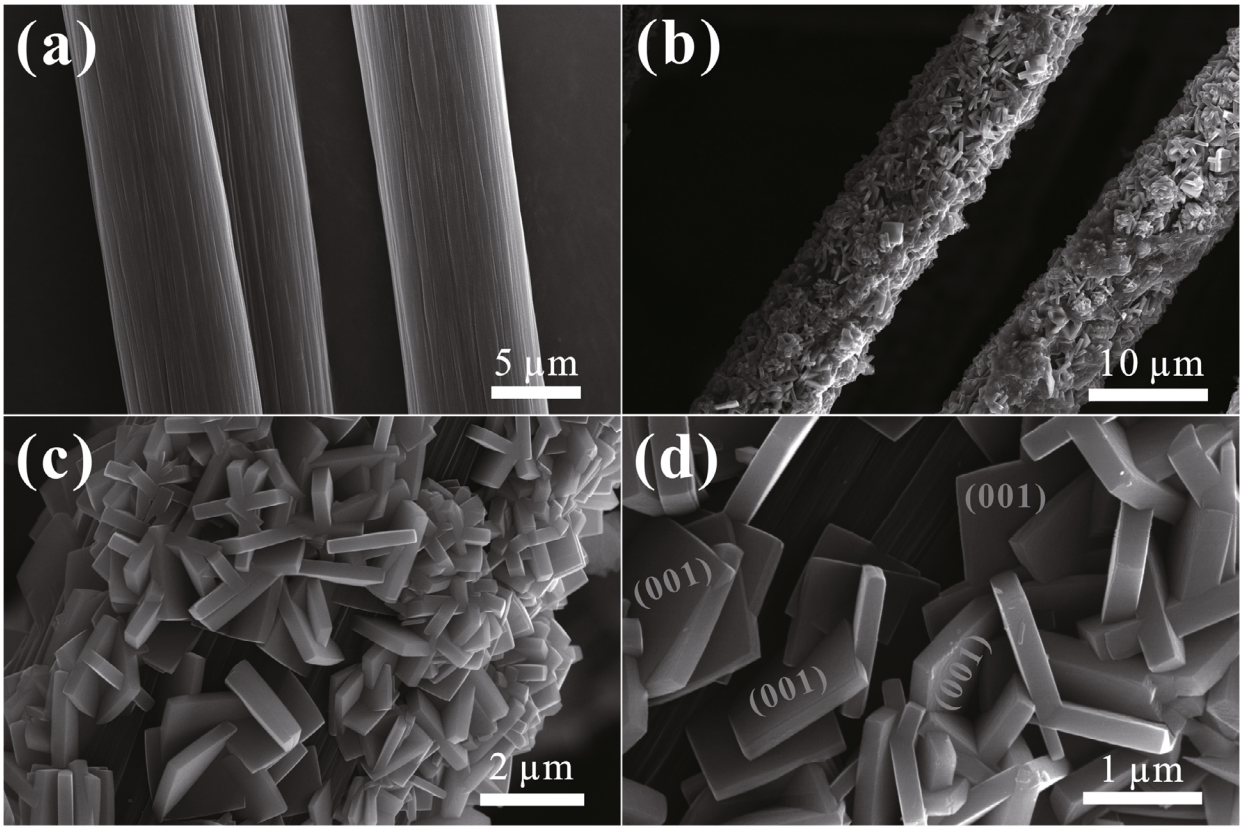


**Fig.15 FESEM images of the carbon fibers (a) and carbon fibers-$TiO_2$ composites (b–d)**

Reprinted with permission (Yang et al., 2019). Copyright 2019, Elsevier.

the larger degree. Through XRD analysis, Li et al. (2017b) concluded that Ag existed in a cubic phase, and as the $TiO_2$ peak remained unchanged, the Ag atom did not enter the $TiO_2$ lattice and replace the Ti. From the typical binding energy of the XPS spectroscopy, it could be concluded that $TiO_2$ was successfully fabricated. Similarly, Liu et al. (2019) also analyzed the characteristic signal of $Ti^{4+}$ and $Sn^{4+}$, which verified that $TiO_2$ and $SnO_2$ were successfully fabricated.

In addition to the above measurements, X-ray photoelectron spectroscopy (XPS) is also a common technology to characterize $TiO_2$ films. XPS uses indefinite carbon to calibrate the binding energy (Yuan and Tsujikawa, 1995; Cui et al., 2015; Hu et al., 2017; Nan et al., 2019). By analyzing the binding

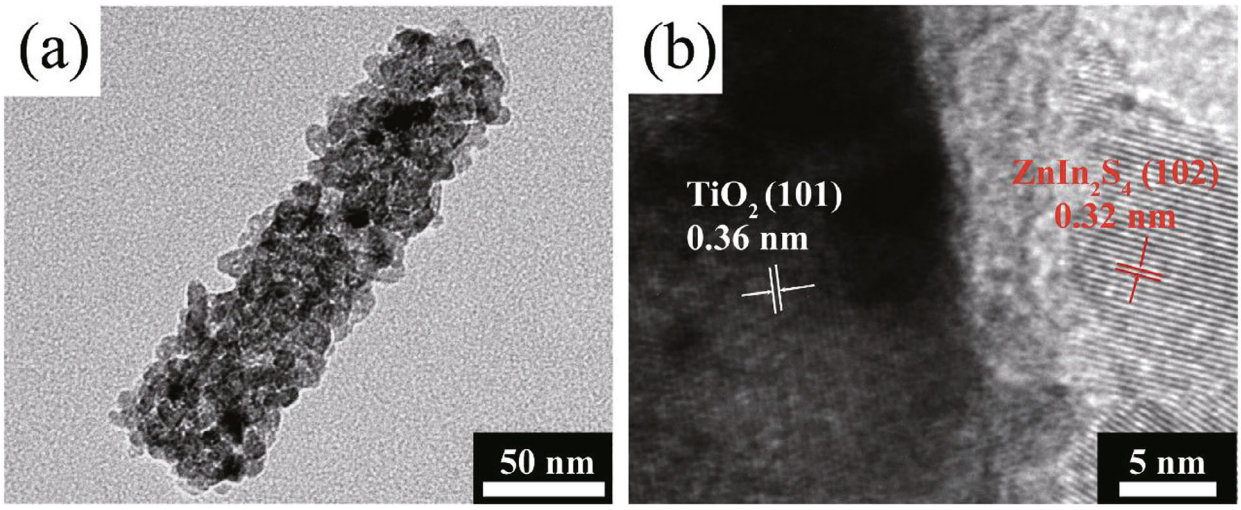


**Fig.16 TEM image (a) and HRTEM image (b) of the $ZnIn_2S_4/TiO_2$ sample**

Reprinted with permission (Li et al., 2019). Copyright 2019, Elsevier.

energy in the diffraction spectroscopy, the element doping and the cohesion between different materials can be determined, as shown in Fig.17.

### 3.2 Photoelectric property test

Photoelectric property tests, including UV-Vis DRS, photoluminescence (PL), and Raman spectroscopy, are significant for photogenerated CP.

Ultraviolet-visible diffuse reflectance spectroscopy (UV-Vis DRS) is used to evaluate optical absorption. Through UV-Vis DRS, it was observed that the absorption edge of pure $TiO_2$ was 380 nm, and the bandgap was calculated to be 3.2 eV. In addition, compared with that of pure $TiO_2$, the increasing absorption of $CdS/TiO_2$ indicated the validity of the modification (Lin et al., 2010). Nan et al. (2019) converted the absorption spectrum of the $Ni_2S_3/TiO_2$ composite film into Tauc plots through the Kubelka-Munk function and found that the band edge of the composite redshifted and the bandgap of $Ni_2S_3$ decreased to 3.1 eV, as illustrated in Fig.18. After examined $TiO_2$ and its composite by UV-Vis DRS, Xie et al. (2019) found that different optical absorption performances for anatase and rutile $TiO_2$ as showed in Fig.18d.

A PL spectroscopy is also capable of certificating the usefulness of modification. For instance, the $CQDs/Ag/TiO_2$ compound has a lower emission intensity than pure $TiO_2$, indicating that fewer photogenerated carriers recombined and generated emission; that is, the conduction of CQDs and Ag contributes to the separation of electrons and holes (Guan et al., 2019). The PL spectroscopy can be analyzed with UV-Vis data to determine the light absorption, as shown in Fig.19.

Similarly, in fluorescence measurements, the fluorescence intensity represents the recombination amount of photoelectrons and holes. Therefore, it is usually used to investigate the photocathodic effect of doping compounds. Xu et al. (2020) noticed that the highest peak position in the fluorescence emission spectroscopy among all samples was approximately 425 nm, and the intensity gradually decreased with the introduction of CdSe, graphene and PANI, which greatly promoted photoelectron-hole separation. The $TiO_2$/CdSe/PANI/graphene (TCPG) composite has a lower fluorescence intensity, which suggests a higher electron-hole pair separation efficiency. Cheng et al. (2017) obtained the fluorescence spectra of $SiO_2/TiO_2$ film, and it was obvious that the compound film had lower fluorescence emission, and the spectra are shown in Fig.20.

In addition, Raman spectra can be used to determine whether the components vary under different treatments. For instance, Bamoulid et al. (2008) observed $TiO_2$ films with different dip times through Raman spectroscopy, and the spectral signature of the surface remained unchanged; thus, the dipping treatment time would not trigger a composition change. Hu et al. (2017) discerned the presence of $Bi_2S_3$ on $TiO_2$ nanotubes through a similar characteristic Raman peak of the specimen with $Bi_2S_3$ deposited on $TiO_2$ and FTO.

### 3.3 Electrochemical test

To investigate and verify the photogenerated CP effect of the photoanodes, electrochemical tests are necessary to examine the potential and current of

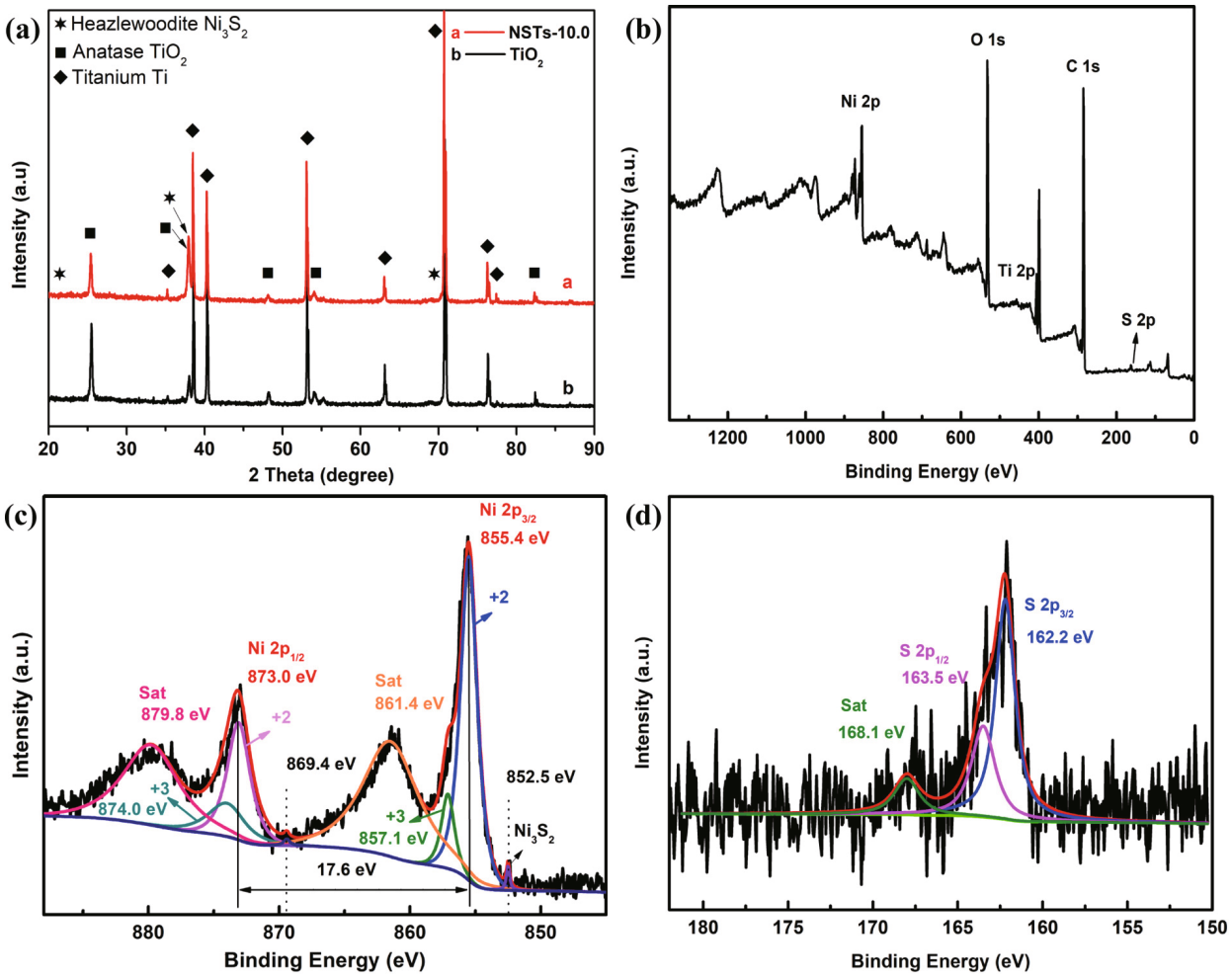


**Fig.17 XRD patterns (a); XPS survey spectra (b); corresponding high-resolution Ni 2p and S 2p XPS spectroscopy of $Ni_3S_2$-doped $TiO_2$ (c & d)**

Reprinted with permission (Nan et al., 2019). Copyright 2019, Elsevier.

stainless steel and the stability of the photoanode. The experiments, including OCP, i-t, EIS, and Mott-Schottky tests, are usually carried out on an electrochemical workstation. The photoelectrochemical cell is usually designed with three electrodes, a working electrode (WE), a counter electrode and SCE as the reference electrode (RE) (Park et al., 2013, Li et al., 2018b), as depicted in Fig.21.

### 3.3.1 OCP and i-t tests

The open circuit potential test and i-t are used to examine the potential and current density with time, respectively. If the potential range is safe for stainless steel, photoanode coupling with a metal can provide protection, and testing the potential for a long time can determine the stability of the photoanode. The OCP and i-t represent the photogenerated charge separation efficiency. In addition, the more negative the OCP is, the higher the i-t, and better the protection. OCP and i-t are usually tested by a three-electrode system on an electrochemical workstation system, such as PARSTAT 4000, CHI660B and Gamry Reference 600. In this system, generally, to simulate a marine environment, 0.5 mol/L (3.5 wt.%) NaCl is placed in the corrosion cell, and the coated metal, SCE and Pt foil are all placed in the NaCl solution as working, reference and counter electrodes, respectively. If the metal is guarded by an independent photoanode, connection remains unchanged and the metal is coupled with the photoanode. In the three-electrode system, to further promote the efficiency of electron and hole separation, $Na_2S$ and NaOH as hole-trapping agents are added to the photoanode cell.

The OCP values of a series of compounds can be compared to determine the composition with optimal photogenerated protection. As shown in the $SiO_2/TiO_2$ compound coupled with 304SS, 10% $SiO_2$ has the most negative potential (-642 mV vs. SCE), 170 mV

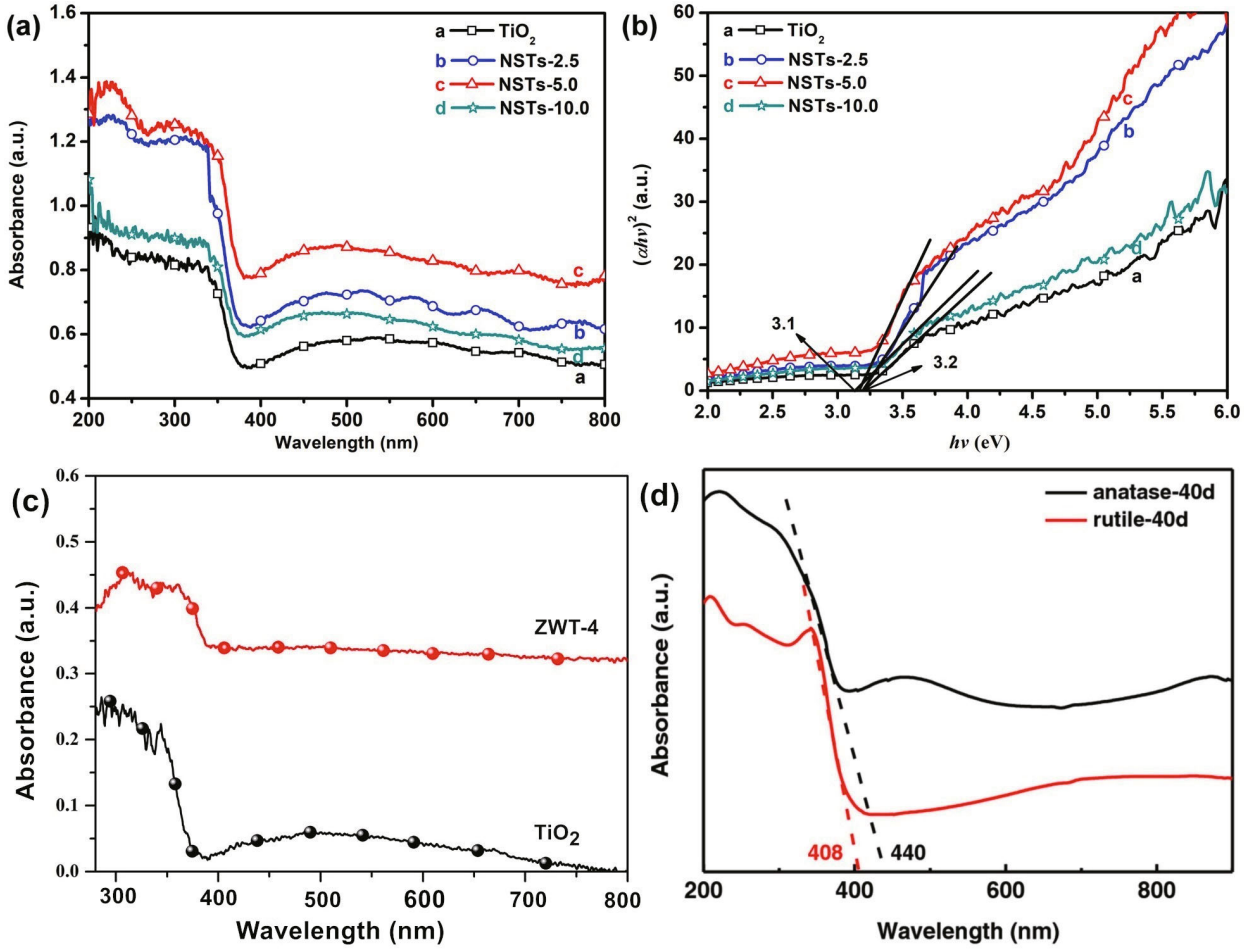


**Fig.18 UV-Vis DRS absorption spectra (a) and Tauc plots of $Ni_3S_2$ nanosheets/$TiO_2$ (b); UV-Vis DRS absorption spectra of $ZnWO_4$/$TiO_2$ (c), and $Co(OH)_2$-modified $TiO_2$ (d)**

a & b. reprinted with permission (Nan et al., 2019). Copyright 2019, Elsevier; c. reprinted with permission (Wang et al., 2019). Copyright 2019, IOP Publishing; d. reprinted with permission (Xie et al. 2018).

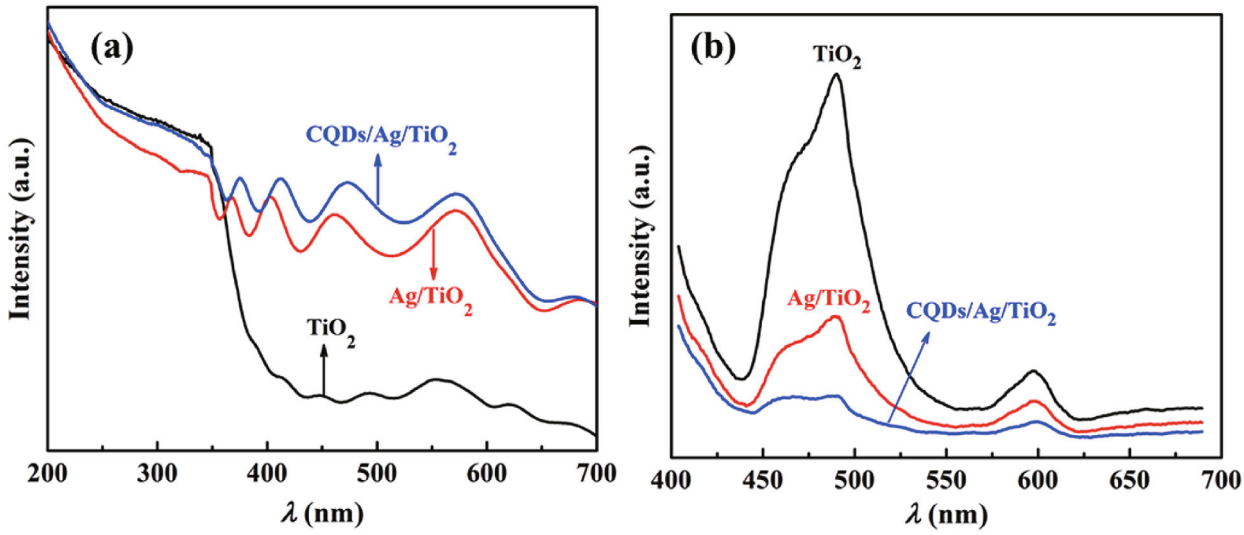


**Fig.19 UV-Vis diffuse reflectance spectroscopy (a) and PL spectra of CQDs/Ag/$TiO_2$ composite film (b)**

Reprinted with permission (Guan et al., 2019). Copyright 2019, Elsevier.

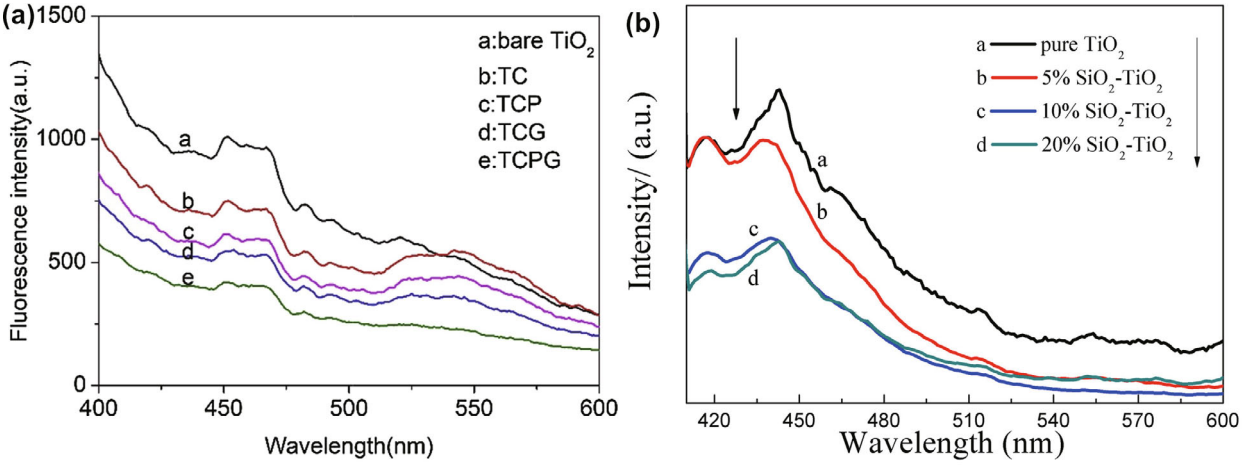


**Fig.20 Fluorescence spectroscopy of the TCPG composite (a) and $SiO_2$-$TiO_2$ film on 304SS (b)**

a. reprinted with permission (Xu et al., 2020). Copyright 2020, Elsevier; b. reprinted with permission (Cheng et al., 2017). Copyright 2017, Elsevier.

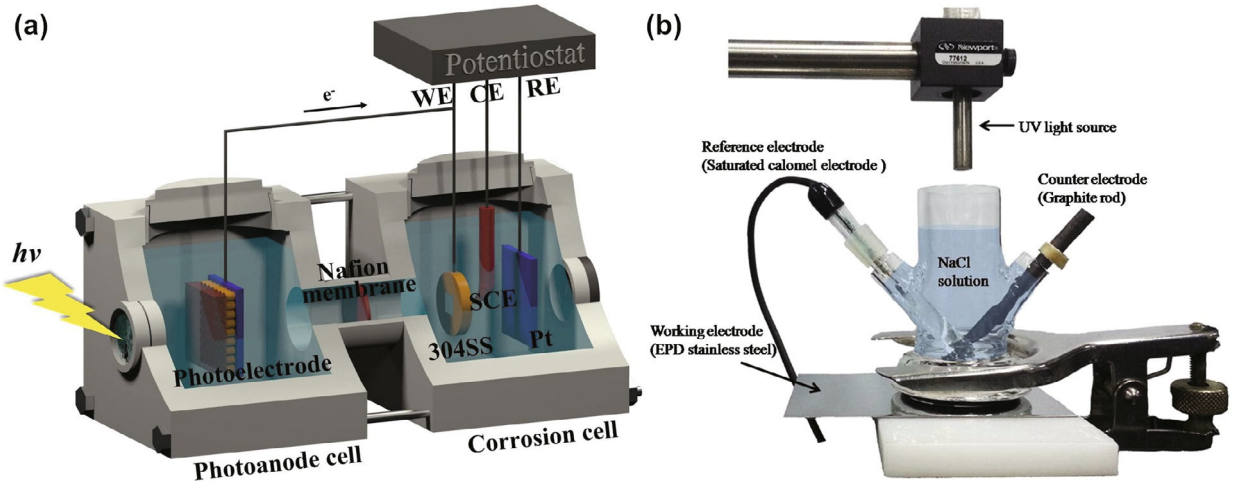


**Fig.21 Photoelectrochemistry cell with three-electrode setup**

a. two cells; b. a single cell. a. reprinted with permission (Li et al., 2018b). Copyright 2018, Elsevier; b. reprinted with permission (Park et al., 2013). Copyright 2013, Elsevier.

lower than that of pure $TiO_2$ (Cheng et al., 2017). The potential for electron transport indicated that $SiO_2$ was instrumental in enhancing the electrochemical properties of $TiO_2$. Park et al. (2013) tested the OCP of coated stainless steel over a long time, and the restoration time of the compound was approximately 6 h after 3 h of irradiation. Under light irradiation, $WO_3$ and $TiO_2$ were excited, electrons were transferred to the metal, and the metal with the $WO_3$/$TiO_2$ coating exhibited a lower potential range of 0.5 V and 0.7 V (vs. SCE) in 3.5 wt.% NaCl. Compared with pure $TiO_2$, $WO_3$ enhanced the photoelectrons and increased the protection time after the simulated light was turned off. After turning off the light, the potential increased slowly to the previous potential in the dark. The transient photocurrent was used to directly evaluate the efficiency of photoelectron and pair separation. Cui et al. (2015) investigated the photocurrent density of 304SS coupled with a PPy/$TiO_2$ nanofilm photoanode. While exposed to the light, the current of PPy/$TiO_2$ increased to 60.5 μA/cm$^2$, and there was no apparent change in the pure $TiO_2$ photoanode. Thus, it could be determined which material has a photocathodic protection effect (Wang et al., 2016a), as shown in Fig.22.

In addition to being used for comparison among composites, OCP can monitor the potential under on-off cycles and long-term illumination. However, the long-term stability and continuous protection performance in the dark are two important factors that affect photocathodic protection, as shown in Fig.23. Hence, long-term OCP measurements are necessary to evaluate the photoelectrochemical properties. Liang et al. (2017) coupled $WO_3$/$TiO_2$ with 403SS

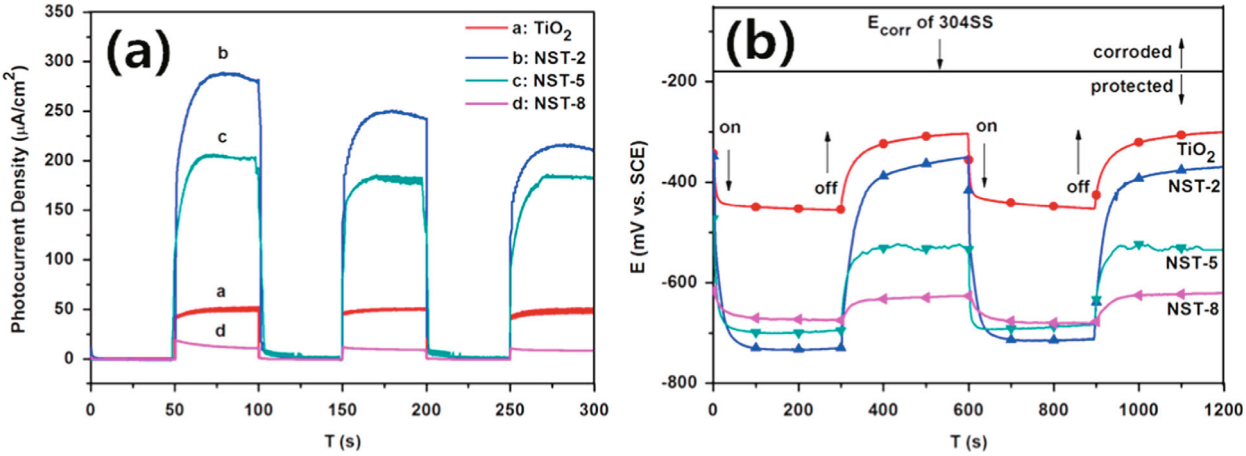


**Fig.22 Photocurrent spectra (a) and OCP of pure $NiSe_2/TiO_2$ nanocomposites (b)**

Reprinted with permission (Wang et al., 2016a). Copyright 2016, Elsevier.

and found that the effective CP lasted for 19 h. Li et al. (2014) set the illumination time as 2 h per cycle, and after turning off the light, the potential of 304SS coupled with Ag and $SnO_2$ cosensitized $TiO_2$ photoanodes remained below the corrosion potential for more than 8 h, which exhibited good durability.

### 3.3.2 EIS and Mott-Schottky measurement

Electrochemical impedance spectroscopy (EIS) shows the electrochemical properties of an electrode and the reaction process at an interface. The Nyquist plots can reflect the electrolyte resistance, coating resistance, coating capacitance, charge transfer resistance, and electrical double layer capacitance of a film and reflect the electron-hole transfer efficiency and the conductance of the film material. Comparing the resistance of different materials can be used to identify better CP. The diameter of the capacitive arc represents the resistance. A large diameter represents high resistance. The Nyquist plot represents a three-element equivalent circuit model, in which the charge transfer resistance and the solution resistance can be represented by Rct and Rs. Furthermore, the small Rct represents a quick electron transfer speed. Zhang et al. (2013) and Guan et al. (2019) verified that the CQDs/Ag/$TiO_2$ composite had a small Rct in the Nyquist plots, which means that a large number of excited photoelectrons flowed to the metal; thus, it was protective for 403SS.

Mott-Schottky measurements can be used to determine the energy band structure and semiconductor type, which provides guidelines for composing materials. Xu et al. (2020) determined the type of $TiO_2$ composites and calculated the flat band according to the slope of the Mott-Schottky spectroscopy, and the reason for the transmission change was further verified; that is, materials with different flat band potentials can be used to construct an internal space electric field that can drive the flow of electrons. The positive slope of the spectra of the different materials implied that pure $TiO_2$ and $Ni_2S_3/TiO_2$ are n-type semiconductors. According to the Mott–Schottky equation, the flat band $E_{fb}$ can be calculated. The deposition of $Ni_2S_3$ is clear. The flat band of the compound shifted negatively; thus, the Fermi level increased, and the conduction band shifted negatively, which indicated an easier and faster transfer efficiency (Nan et al., 2019). The EIS and Mott-Schottky analyses are shown in Fig.24.

### 3.3.3 i-v and Tafel test

In addition, there are also other analysis techniques, such as i-v and the Tafel method. In photoelectrochemical anticorrosion research, the Tafel polarization curve is used to recognize the corrosion potential and current. Linear sweep voltammetry can be used to measure the threshold bias potential, which is the crucial potential corresponding to the occurrence of photoanodes and related to the reducing ability. Li et al. (2018a) investigated i-v tests for $TiO_2$ and the $Sb_2S_3/Sb_2O_3/TiO_2$ composites and found that the composite had a more negative potential, stronger reduction capacity, higher photocurrent and more efficient transfer ability.

The Tafel curve reflects the polarization process, and the corrosion current density can be easily obtained from the curve. Zhou et al. (2009) tested the corrosion current and found that 304SS coupled with $WO_3/TiO_2$ had a more negative potential than pure 304SS under illumination. Zuo et al. (2018) verified

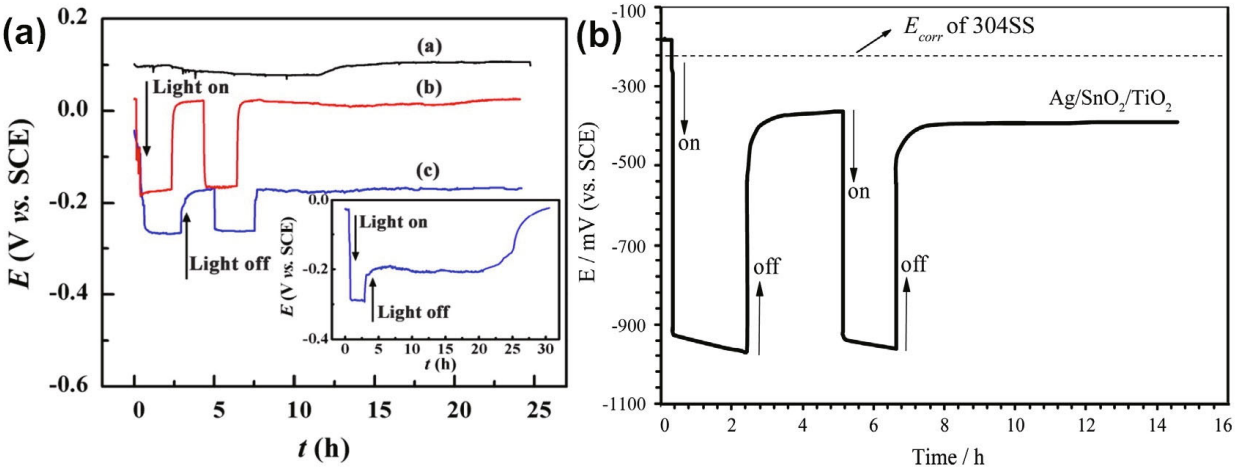


**Fig.23 Long-term OCP variations of metal coupled with $WO_3/TiO_2$ (a) and $Ag/SnO_2/TiO_2$ (b)**

a. reprinted with permission (Liang et al., 2017). Copyright 2017, Elsevier; b. reprinted with permission (Li et al., 2014). Copyright 2014, Elsevier.

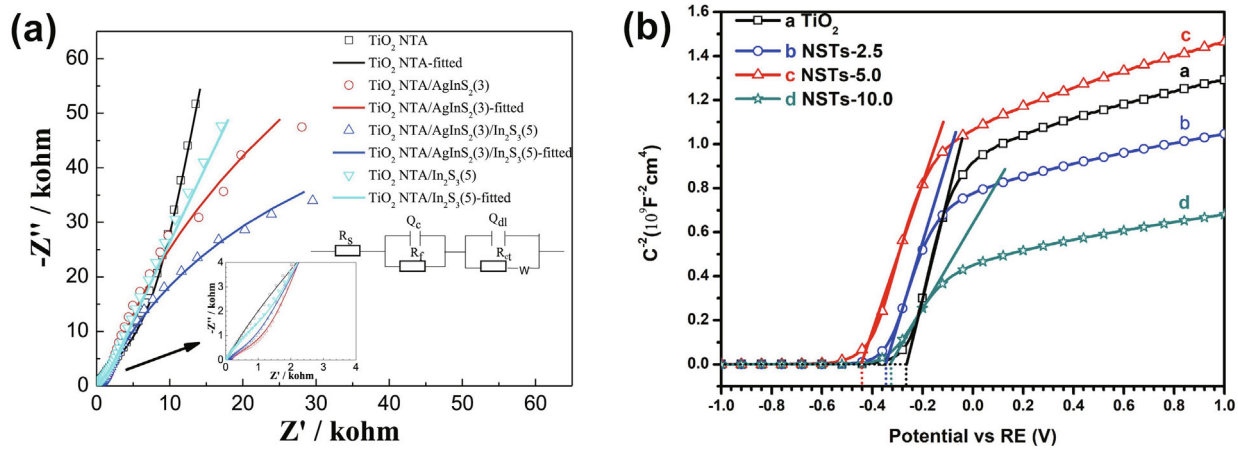


**Fig.24 Nyquist plots of $AgInS_2/In_2S_3$-doped $TiO_2$ NTAs (a) and Mott-Schottky plots of $Ni_3S_2$-doped $TiO_2$ (b)**

a. reprinted with permission (Sun et al., 2018a). Copyright 2018, Elsevier; b. reprinted with permission (Nan et al., 2019). Copyright 2019, Elsevier.

that the flower-like nanostructure had the best corrosion protection performance among nanorods, nanospheres and flower-like nanostructures because it had the most negative potential and the highest current in the Tafel curve, as shown in Fig.25.

### 3.4 Characterization of metal

Although there are many characterization and test methods to verify the protection effect of $TiO_2$, it is important to view the real anticorrosion degree in a simulated marine environment and monitor the surface of stainless steel in real time.

Optical microscopy was used to observe the corrosion morphology change of metals after testing (Mahmoud et al., 2005). Direct observation can be used to verify the credibility of previous outcomes. Xu et al. (2020) analyzed the surface morphology of 304SS through optical microscopy after different corrosion times. Many corrosion pits could be seen on the surface of 304SS without protection. After coupling with $TiO_2$ photoanodes, the quantity and size of the pits decreased.

When testing the protection of ZnO and $TiO_2$ layers on 304SS, Boukerche et al. (2019) found through optical microscopy that ZnO and $TiO_2$ films with different proportions had different colors, which provided the ability to discern the features of films. Li and Fu (2013) observed the morphology after accelerated corrosion tests, which were conducted for 316L stainless steel substrates with chromium-doped $TiO_2$ coatings, and found that the photocathodic protection was increased by using chromium doping. Xie et al. (2019) compared the protection of Q235 steel with $Co(OH)_2$-modified $TiO_2$ to that of traditional sacrificial anodes in 3.5 wt.% NaCl solution for 15 days and investigated the macrocorrosion

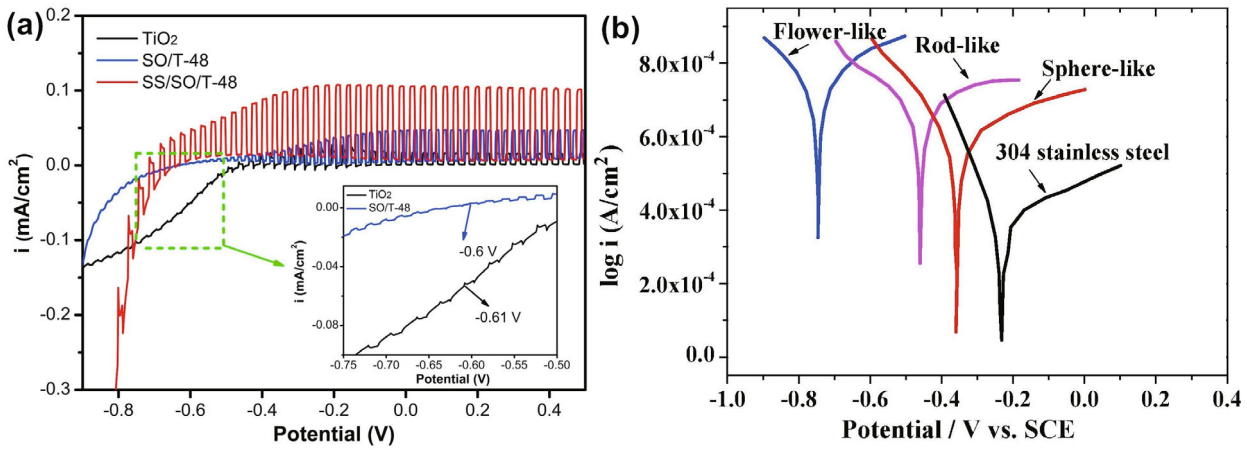


**Fig.25 Photoinduced i-v curve of the $Sb_2S_3/Sb_2O_3/TiO_2$ composites (a) and Tafel polarization curves of 304 stainless steel coupled with different $TiO_2$ (b)**

a. reprinted with permission (Li et al., 2018b). Copyright 2018, Elsevier; b. reprinted with permission (Liang et al., 2018). Copyright 2018, Elsevier.

morphologies of the steel, as shown in Fig.26. The experiments proved that the photoanode composites provided effective supplemental protection for steel.

To explore the detailed morphology of the metal under the protection of photoanodes with light irradiation, SEM was employed for further investigation. Liu et al. (2014) found that the SEM images of 304SS showed that some corrosion pits emerged on the surface after dipping the samples in 0.5 mol/L NaCl solutions without photocathodic protection and that no pits were observed on the surface of 304SS coupled with an Fe-doped $TiO_2$ photoanode, as shown in Fig.27.

## 4 SUMMARY AND PERSPECTIVE

Photocathodic protection is a promising technology for metal corrosion in marine environment. The present review shows the application of $TiO_2$ and its modification to prevent corrosion. Nevertheless, two defects limit the widespread application of $TiO_2$: low absorption of visible light and quick recombination of photogenerated carriers. In the past 25 years, much progress has been achieved in this field, and different nanostructures with doping, modification and band construction have been developed to improve the photocatalytic performance of $TiO_2$. There is still a large potential to promote the utilization of sunlight.

More characterization and analysis are needed to increase the understanding of the fundamental and kinetic processes of photocathodic protection. For example, density functional theory calculations can help design composite materials and determine the mechanism of the process. However, crucial problems still exist in the application of photocathodic protection. To effectively promote the separation of electrons and holes, sacrificial agents such as $Na_2S$, NaOH and $Na_2SO_4$ are usually added to the solution, and much effort has been made to substitute the sacrificial agents. Another challenge is achieving continuous protection in a dark environment. Although energy storage materials have increased protection without visible light irradiation, the development of new green energy materials with low cost is still needed. $TiO_2$-based composite materials will play an important role in the photocathodic protection field.

However, to improve the photocathodic protection performance, a wider range of new materials and new technologies should be investigated. For example, MXenes and MOFs can be constructed into 2D nanosheets (Guan and Han, 2019), and physical vapor deposition and chemical vapor deposition (Muratore et al., 2019) can also be used. Combining photocathodic protection with sacrificial anode protection or new energy harvesting technology, such as triboelectric nanogenerators, can harvest wave energy (Feng et al., 2016) and mechanical energy (Yang et al., 2020) and provide more effective protection for metals. Thus, it is expected that the combination of photocathodic protection and triboelectric nanogenerators will be of use in anticorrosion technologies.

## 5 DATA AVAILABILITY STATEMENT

Data sharing not applicable to this article as no datasets were generated or analysed during the current study.

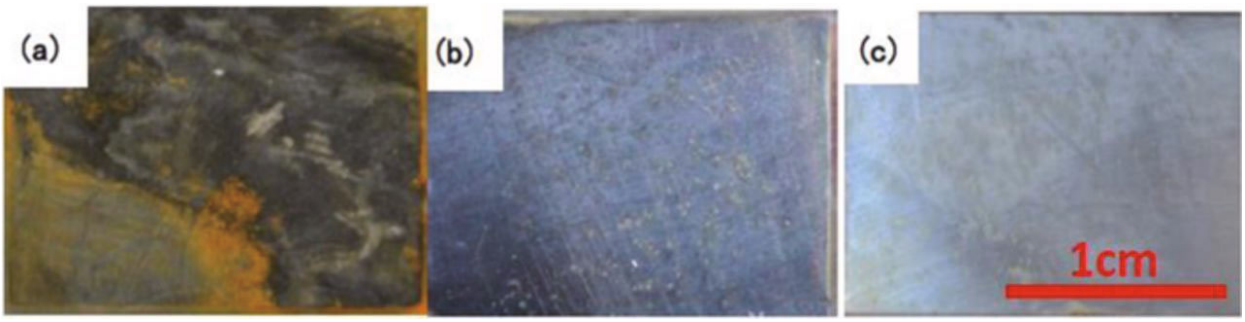


**Fig.26 Corrosion morphologies of Q235 unprotected (a), protected (b) by SACP and protected by Al photoanode composite (c)**

a, b, c. reprinted with permission (Xie et al. 2019).

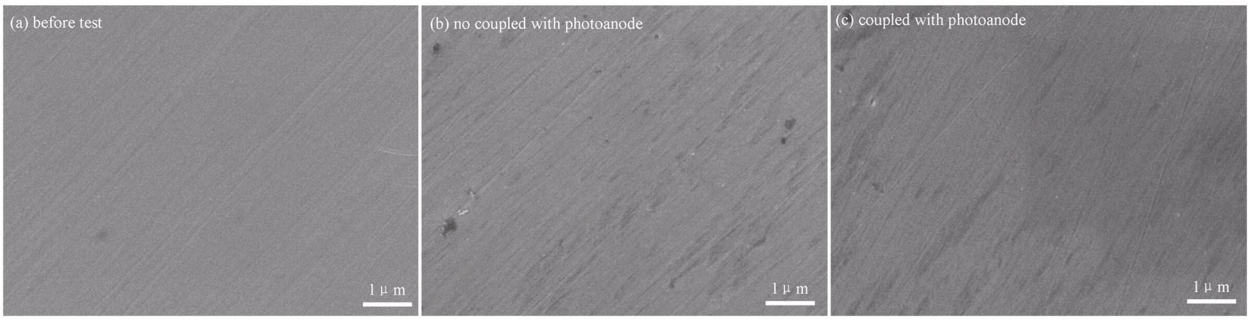


**Fig.27 SEM images of 304SS blank (a); no protection (b); and coupled with Fe-doped $TiO_2$ (c)**

Reprinted with permission (Liu et al., 2014). Copyright 2014, Elsevier.

## References


Balaur E, Macak J M, Taveira L, Schmuki P. 2005. Tailoring the wettability of $TiO_2$ nanotube layers. *Electrochemistry Communications*, **7**(10): 1 066-1 070, https://doi.org/10.1016/j.elecom.2005.07.014.

Bamoulid L, Maurette M T, De Caro D, Guenbour A, Ben Bachir A, Aries L, El Hajjaji S, Benoît-Marquié F, Ansart F. 2008. An efficient protection of stainless steel against corrosion: combination of a conversion layer and titanium dioxide deposit. *Surface and Coatings Technology*, **202**(20): 5 020-5 026, https://doi.org/10.1016/j.surfcoat.2008.05.011.

Boonserm A, Kruehong C, Seithtanabutara V, Artnaseaw A, Kwakhong P. 2017. Photoelectrochemical response and corrosion behavior of $CdS/TiO_2$ nanocomposite films in an aerated 0.5 M NaCl solution. *Applied Surface Science*, **419**: 933-941, https://doi.org/10.1016/j.apsusc.2017.05.093.

Boukerche S, Himour A, Bououdina M, Bensouici F, Ouchenane S. 2019. Multilayered $ZnO/TiO_2$ nanostructures as efficient corrosion protection for stainless steel 304. *Materials Research Express*, **6**(5): 055052, https://doi.org/10.1088/2053-1591/ab042f.

Bu Y Y, Chen Z Y, Ao J P, Hou J, Sun M X. 2018. Study of the photoelectrochemical cathodic protection mechanism for steel based on the $SrTiO_3$-$TiO_2$ composite. *Journal of Alloys and Compounds*, **731**: 1 214-1 224, https://doi.org/10.1016/j.jallcom.2017.10.165.

Bu Y Y, Chen Z Y, Yu J Q, Li W B. 2013. A novel application of g-$C_3N_4$ thin film in photoelectrochemical anticorrosion. *Electrochimica Acta*, **88**: 294-300, https://doi.org/10.1016/j.electacta.2012.10.049.

Bu Y Y, Li W B, Yu J Q, Wang X T, Qi M L, Nie M Y, Hou B R. 2011. Fabrication of $SrTiO_3$ nanocrystalline film photoelectrode and its photoelectrochemical anticorrosion properties for stainless steel. *Acta Physico-Chimica Sinica*, **27**(10): 2 393-2 399, https://doi.org/10.3866/PKU.WHXB20110926. (in Chinese with English abstract)

Cai J S, Shen J L, Zhang X N, Ng Y H, Huang J Y, Guo W X, Lin C J, Lai Y K. 2019. Light-driven sustainable hydrogen production utilizing $TiO_2$ nanostructures: a review. *Small Methods*, **3**(1): 1800184, https://doi.org/10.1002/smtd.201800184.

Chen J S, Tan Y L, Li C M, Cheah Y L, Luan D Y, Madhavi S, Boey F Y C, Archer L A, Lou X W. 2010. Constructing hierarchical spheres from large ultrathin anatase $TiO_2$ Nanosheets with nearly 100% exposed (001) facets for fast reversible lithium storage. *Journal of the American Chemical Society*, **132**(17): 6 124-6 130, https://doi.org/10.1021/ja100102y.

Chen X B, Li C, Grätzel M, Kostecki R, Mao S S. 2012. Nanomaterials for renewable energy production and storage. *Chemical Society Reviews*, **41**(23): 7 909-7 937, https://doi.org/10.1039/c2cs35230c.

Chen Z H, Yang W Z, Xu B, Chen Y, Qian M Q, Su X, Li Z H, Yin X S, Liu Y. 2019. Corrosion protection of carbon steels by electrochemically synthesized V-$TiO_2$/polypyrrole composite coatings in 0.1 M HCl solution. *Journal of Alloys and Compounds*, **771**: 857-868, https://

doi.org/10.1016/j.jallcom.2018.09.003.

Cheng W H, Li C D, Ma X, Yu L M, Liu G Y. 2017. Effect of $SiO_2$-doping on photogenerated cathodic protection of nano-$TiO_2$ films on 304 stainless steel. *Materials & Design*, **126**: 155-161, https://doi.org/10.1016/j.matdes.2017.04.041.

Cui J, Pei Y S. 2019. Enhanced photocathodic protection performance of $Fe_2O_3/TiO_2$ heterojunction for carbon steel under simulated solar light. *Journal of Alloys and Compounds*, **779**: 183-192, https://doi.org/10.1016/j.jallcom.2018.11.281.

Cui S W, Yin X Y, Yu Q L, Liu Y P, Wang D A, Zhou F. 2015. Polypyrrole nanowire/$TiO_2$ nanotube nanocomposites as photoanodes for photocathodic protection of Ti substrate and 304 stainless steel under visible light. *Corrosion Science*, **98**: 471-477, https://doi.org/10.1016/j.corsci.2015.05.059.

Davy H. 1824. On the corrosion of copper sheeting by sea water, and on methods of preventing this effect, and on their application to ships of war and other ships. *Philosophical Transactions*, **114**: 151-158, https://doi.org/10.1098/rstl.1824.0009.

Deng H D, Huang M C, Weng W H, Lin J C. 2015. Photocathodic protection of iron oxide nanotube arrays fabricated on carbon steel. *Surface and Coatings Technology*, **266**: 183-187, https://doi.org/10.1016/j.surfcoat.2015.02.042.

Ding D, Hou Q K, Su Y G, Li Q Q, Liu L, Jing J, Lin B, Chen Y. 2019. g-$C_3N_4/TiO_2$ hybrid film on the metal surface, a cheap and efficient sunlight active photoelectrochemical anticorrosion coating. *Journal of Materials Science*: *Materials in Electronics*, **30**(13): 12 710-12 717, https://doi.org/10.1007/s10854-019-01635-z.

Feng Y G, Zheng Y B, Rahman Z U, Wang D A, Zhou F, Liu W M. 2016. Paper-based triboelectric nanogenerators and their application in self-powered anticorrosion and antifouling. *Journal of Materials Chemistry A*, **4**(46): 18 022-18 030, https://doi.org/10.1039/c6ta07288g.

Fujishima A, Honda K. 1972. Electrochemical photolysis of water at a semiconductor electrode. *Nature*, **238**(5358): 37-38, https://doi.org/10.1038/238037a0.

Fujishima A, Zhang X T, Tryk D A. 2008. $TiO_2$ photocatalysis and related surface phenomena. *Surface Science Reports*, **63**(12): 515-582, https://doi.org/10.1016/j.surfrep.2008.10.001.

Ge S S, Zhang Q X, Wang X T, Li H, Zhang L, Wei Q Y. 2015. Photocathodic protection of 304 stainless steel by MnS/$TiO_2$ nanotube films under simulated solar light. *Surface and Coatings Technology*, **283**: 172-176, https://doi.org/10.1016/j.surfcoat.2015.10.061.

Guan G J, Han M Y. 2019. Functionalized hybridization of 2D nanomaterials. *Advanced Science*, **6**(23): 1901837, https://doi.org/10.1002/advs.201901837.

Guan Z C, Jin P, Liu Q, Wang X, Chen L F, Xu H, Song G L, Du R G. 2019. Carbon quantum dots/Ag sensitized $TiO_2$ nanotube film for applications in photocathodic protection. *Journal of Alloys and Compounds*, **797**: 912-921, https://doi.org/10.1016/j.jallcom.2019.05.199.

Guan Z C, Wang H P, Wang X, Hu J, Du R G. 2018a. Fabrication of heterostructured β-$Bi_2O_3$-$TiO_2$ nanotube array composite film for photoelectrochemical cathodic protection applications. *Corrosion Science*, **136**: 60-69, https://doi.org/10.1016/j.corsci.2018.02.048.

Guan Z C, Wang X, Jin P, Tang Y Y, Wang H P, Song G L, Du R G. 2018b. Enhanced photoelectrochemical performances of ZnS-$Bi_2S_3/TiO_2/WO_3$ composite film for photocathodic protection. *Corrosion Science*, **143**: 31-38, https://doi.org/10.1016/j.corsci.2018.07.037.

Guo Q, Zhou C Y, Ma Z B, Yang X M. 2019. Fundamentals of $TiO_2$ photocatalysis: concepts, mechanisms, and challenges. *Advanced Materials*, **31**(50): 1901997, https://doi.org/10.1002/adma.201901997.

Hou B R, Li X G, Ma X M, Du C W, Zhang D W, Zheng M, Xu W C, Lu D Z, Ma F B. 2017. The cost of corrosion in China. *npj Materials Degradation*, **1**(1): 4, https://doi.org/10.1038/s41529-017-0005-2.

Hou B R. 2019. Introduction to *a study on corrosion status and control strategies in China*. *In*: Hou B R ed. The Cost of Corrosion in China. Springer, Singapore. p.1-33, https://doi.org/10.1007/978-981-32-9354-0_1.

Hu J, Guan Z C, Liang Y, Zhou J Z, Liu Q, Wang H P, Zhang H, Du R G. 2017. $Bi_2S_3$ modified single crystalline rutile $TiO_2$ nanorod array films for photoelectrochemical cathodic protection. *Corrosion Science*, **125**: 59-67, https://doi.org/10.1016/j.corsci.2017.06.003.

Hu J, Liu Q, Zhang H, Chen C D, Liang Y, Du R G, Lin C J. 2015a. Facile ultrasonic deposition of $SnO_2$ nanoparticles on $TiO_2$ nanotube films for enhanced photoelectrochemical performances. *Journal of Materials Chemistry A*, **3**(45): 22 605-22 613, https://doi.org/10.1039/c5ta06752a.

Hu J, Zhu Y F, Liu Q, Gao Y B, Du R G, Lin C J. 2015b. $SnO_2$ nanoparticle films prepared by pulse current deposition for photocathodic protection of stainless steel. *Journal of the Electrochemical Society*, **162**(4): C161-C166, https://doi.org/10.1149/2.0451504jes.

Huang J S, Shinohara T, Tsujikawa S. 2000. Photoeffect on corrosion behavior of $SrTiO_3$-coated galvanized steel. *Zairyo-to-Kankyo*, **49**(10): 625-631, https://doi.org/10.3323/jcorr1991.49.625.

Jing J P, Chen Z Y, Bu Y Y, Xu L K. 2016. Photoelectrochemical cathodic protection induced from nanoflower-structured $WO_3$ sensitized with CdS nanoparticles. *Journal of the Electrochemical Society*, **163**(14): C928-C936, https://doi.org/10.1149/2.0141702jes.

Kudo A, Miseki Y. 2009. Heterogeneous photocatalyst materials for water splitting. *Chemical Society Reviews*, **38**(1): 253-278, https://doi.org/10.1039/b800489g.

Lan K, Liu Y, Zhang W, Liu Y, Elzatahry A, Wang R C, Xia Y Y, Al-Dhayan D, Zheng N F, Zhao D Y. 2018. Uniform ordered two-dimensional mesoporous $TiO_2$ nanosheets from hydrothermal-induced solvent-confined monomicelle assembly. *Journal of the American Chemical Society*, **140**(11): 4 135-4 143, https://doi.org/10.1021/jacs.8b00909.

Lei C X, Liu Y, Zhou H, Feng Z D, Du R G. 2013. Photogenerated cathodic protection of stainless steel by liquid-phase-deposited sodium polyacrylate/$TiO_2$ hybrid films. *Corrosion Science*, **68**: 214-222, https://doi.org/10.1016/j.corsci.2012.11.019.

Lei C X, Zhou H, Feng Z D, Zhu Y F, Du R G. 2012. Liquid phase deposition (LPD) of $TiO_2$ thin films as photoanodes for cathodic protection of stainless steel. *Journal of Alloys and Compounds*, **513**: 552-558, https://doi.org/10.1016/j.jallcom.2011.11.005.

Lenz D M, Delamar M, Ferreira C A. 2003. Application of polypyrrole/$TiO_2$ composite films as corrosion protection of mild steel. *Journal of Electroanalytical Chemistry*, **540**: 35-44, https://doi.org/10.1016/s0022-0728(02)01272-x.

Li H, Li Y H, Wang M, Niu Z, Wang X T, Hou B R. 2018a. Preparation and photocathodic protection property of $ZnIn_2S_4$/RGO/$TiO_2$ composites for Q235 carbon steel under visible light. *Nanotechnology*, **29**(43): 435706, https://doi.org/10.1088/1361-6528/aada28.

Li H, Li Y H, Wang X T, Hou B R. 2019. 3D $ZnIn_2S_4$ nanosheets/$TiO_2$ nanotubes as photoanodes for photocathodic protection of Q235 CS with high efficiency under visible light. *Journal of Alloys and Compounds*, **771**: 892-899, https://doi.org/10.1016/j.jallcom.2018.09.027.

Li H, Wang X T, Liu Y, Hou B R. 2014. Ag and $SnO_2$ co-sensitized $TiO_2$ photoanodes for protection of 304SS under visible light. *Corrosion Science*, **82**: 145-153, https://doi.org/10.1016/j.corsci.2014.01.009.

Li H, Wang X T, Wei Q Y, Hou B R. 2017a. Photocathodic protection of 304 stainless steel by $Bi_2S_3$/$TiO_2$ nanotube films under visible light. *Nanoscale Research Letters*, **12**(1): 80, https://doi.org/10.1186/s11671-017-1863-9.

Li H, Wang X T, Wei Q Y, Liu X Q, Qian Z H, Hou B R. 2017b. Enhanced photocathodic protection performance of Ag/graphene/$TiO_2$ composite for 304SS under visible light. *Nanotechnology*, **28**(22): 225701, https://doi.org/10.1088/1361-6528/aa6e5d.

Li H, Wang X T, Zhang L, Hou B R. 2015a. CdTe and graphene co-sensitized $TiO_2$ nanotube array photoanodes for protection of 304SS under visible light. *Nanotechnology*, **26**(15): 155704, https://doi.org/10.1088/0957-4484/26/15/155704.

Li H, Wang X T, Zhang L, Hou B R. 2015b. Preparation and photocathodic protection performance of CdSe/reduced graphene oxide/$TiO_2$ composite. *Corrosion Science*, **94**: 342-349, https://doi.org/10.1016/j.corsci.2015.02.017.

Li J T, Wu N Q. 2015. Semiconductor-based photocatalysts and photoelectrochemical cells for solar fuel generation: a review. *Catalysis Science & Technology*, **5**(3): 1 360-1 384, https://doi.org/10.1039/c4cy00974f.

Li J, Lin C J, Lai Y K, Du R G. 2010. Photogenerated cathodic protection of flower-like, nanostructured, N-doped $TiO_2$ film on stainless steel. *Surface and Coatings Technology*, **205**(2): 557-564, https://doi.org/10.1016/j.surfcoat.2010.07.030.

Li J, Lin C J, Li J T, Lin Z Q. 2011. A photoelectrochemical study of CdS modified $TiO_2$ nanotube arrays as photoanodes for cathodic protection of stainless steel. *Thin Solid Films*, **519**(16): 5 494-5 502, https://doi.org/10.1016/j.tsf.2011.03.116.

Li J, Yun H, Lin C J. 2007. The Fe-doped $TiO_2$ nanotube arrays as a photoanode for cathodic protection of stainless steel. *Acta Physico-Chimica Sinica*, **23**(12): 1 886-1 892, https://doi.org/10.3866/pku.Whxb20071211. (in Chinese with English abstract)

Li S N, Fu J J. 2013. Improvement in corrosion protection properties of $TiO_2$ coatings by chromium doping. *Corrosion Science*, **68**: 101-110, https://doi.org/10.1016/j.corsci.2012.10.040.

Li S N, Wang Q, Chen T, Zhou Z H, Wang Y, Fu J J. 2012. Study on cerium-doped nano-$TiO_2$ coatings for corrosion protection of 316 L stainless steel. *Nanoscale Research Letters*, **7**(1): 227, https://doi.org/10.1186/1556-276x-7-227.

Li X R, Wang X T, Ning X B, Lei J, Shao J, Wang W C, Huang Y L, Hou B R. 2018b. $Sb_2S_3$/$Sb_2O_3$ modified $TiO_2$ photoanode for photocathodic protection of 304 stainless steel under visible light. *Applied Surface Science*, **462**: 155-163, https://doi.org/10.1016/j.apsusc.2018.08.108.

Liang Y, Guan Z C, Wang H P, Du R G. 2017. Enhanced photoelectrochemical anticorrosion performance of $WO_3$/$TiO_2$ nanotube composite films formed by anodization and electrodeposition. *Electrochemistry Communications*, **77**: 120-123, https://doi.org/10.1016/j.elecom.2017.03.008.

Lin Z Q, Lai Y K, Hu R G, Li J, Du R G, Lin C J. 2010. A highly efficient ZnS/CdS@$TiO_2$ photoelectrode for photogenerated cathodic protection of metals. *Electrochimica Acta*, **55**(28): 8 717-8 723, https://doi.org/10.1016/j.electacta.2010.08.017.

Linsebigler A L, Lu G Q, Yates J T. 1995. Photocatalysis on $TiO_2$ surfaces: principles, mechanisms, and selected results. *Chemical Reviews*, **95**(3): 735-758, https://doi.org/10.1021/cr00035a013.

Liu L, Hu J M, Leng W H, Zhang J Q, Cao C N. 2007. Novel bis-silane/$TiO_2$ bifunctional hybrid films for metal corrosion protection both under ultraviolet irradiation and in the dark. *Scripta Materialia*, **57**(6): 549-552, https://doi.org/10.1016/j.scriptamat.2007.04.044.

Liu W J, Du T, Ru Q X, Zuo S X, Cai Y H, Yao C. 2018. Preparation of graphene/$WO_3$/$TiO_2$ composite and its photocathodic protection performance for 304 stainless steel. *Materials Research Bulletin*, **102**: 399-405, https://doi.org/10.1016/j.materresbull.2018.03.012.

Liu W J, Yin K C, He F, Ru Q X, Zuo S X, Yao C. 2019. A highly efficient reduced graphene oxide/$SnO_2$/$TiO_2$ composite as photoanode for photocathodic protection of 304 stainless steel. *Materials Research Bulletin*, **113**: 6-13, https://doi.org/10.1016/j.materresbull.2018.12.039.

Liu Y, Xu C, Feng Z D. 2014. Characteristics and anticorrosion performance of Fe-doped $TiO_2$ films by liquid phase deposition method. *Applied Surface Science*, **314**: 392-399, https://doi.org/10.1016/j.apsusc.2014.07.042.

Lu X Y, Liu L, Xie X, Cui Y, Oguzie E E, Wang F H. 2020. Synergetic effect of graphene and $Co(OH)_2$ as cocatalysts of $TiO_2$ nanotubes for enhanced photogenerated cathodic protection. *Journal of Materials Science & Technology*, **37**: 55-63, https://doi.org/10.1016/j.jmst.2019.07.034.

Ma Z, Ma X M, Liu N Z, Wang X T, Wang L F, Hou B R. 2020. Study on the photocathodic protection of 304 stainless steel by Ag and $In_2S_3$ co-sensitized $TiO_2$ composite. *Applied Surface Science*, **507**: 145088, https://doi.org/10.1016/j.apsusc.2019.145088.

Mahmoud M G, Wang R G, Kato M, Nakasa K. 2005. Influence of ultraviolet light irradiation on corrosion behavior of weathering steel with and without $TiO_2$-coating in 3 mass% NaCl solution. *Scripta Materialia*, **53**(11): 1 303-1 308, https://doi.org/10.1016/j.scriptamat.2005.07.039.

Matsunaga T, Tomoda R, Nakajima T, Nakamura N, Komine T. 1988. Continuous-sterilization system that uses photosemiconductor powders. *Applied and Environmental Microbiology*, **54**(6): 1 330-1 333.

Melchers R E. 2003. Modeling of marine immersion corrosion for mild and low-alloy steels — Part 1: phenomenological model. *Corrosion*, **59**(4): 319-334, https://doi.org/10.5006/1.3277564.

Momeni M M, Ghayeb Y, Moosavi N. 2018. Preparation of Ni-Pt/Fe-$TiO_2$ nanotube films for photoelectrochemical cathodic protection of 403 stainless steel. *Nanotechnology*, **29**(42): 425701, https://doi.org/10.1088/1361-6528/aad5f5.

Muratore C, Voevodin A A, Glavin N R. 2019. Physical vapor deposition of 2D Van der Waals materials: a review. *Thin Solid Films*, **688**: 137500, https://doi.org/10.1016/j.tsf.2019.137500.

Nagaveni K, Sivalingam G, Hegde M S, Madras G. 2004. Solar photocatalytic degradation of dyes: high activity of combustion synthesized nano $TiO_2$. *Applied Catalysis B*: *Environmental*, **48**(2): 83-93, https://doi.org/10.1016/j.apcatb.2003.09.013.

Nan Y B, Wang X T, Ning X B, Lei J, Guo S Y, Huang Y L, Duan J Z. 2019. Fabrication of $Ni_3S_2/TiO_2$ photoanode material for 304 stainless steel photocathodic protection under visible light. *Surface and Coatings Technology*, **377**: 124935, https://doi.org/10.1016/j.surfcoat.2019.124935.

Ning X B, Ge S S, Wang X T, Li H, Li X R, Liu X Q, Huang Y L. 2017. Preparation and photocathodic protection property of $Ag_2S$-$TiO_2$ composites. *Journal of Alloys and Compounds*, **719**: 15-21, https://doi.org/10.1016/j.jallcom.2017.05.133.

Oh S H, Finõnes R R, Daraio C, Chen L H, Jin S. 2005. Growth of Nano-scale hydroxyapatite using chemically treated titanium oxide nanotubes. *Biomaterials*, **26**(24): 4 938-4 943, https://doi.org/10.1016/j.biomaterials.2005.01.048.

Ohko Y, Saitoh S, Tatsuma T, Fujishima A. 2001. Photoelectrochemical anticorrosion and self-cleaning effects of a $TiO_2$ coating for type 304 stainless steel. *Journal of the Electrochemical Society*, **148**(1): B24-B28, https://doi.org/10.1149/1.1339030.

O'Regan B, Grätzel M. 1991. A low-cost, high-efficiency solar cell based on dye-sensitized colloidal $TiO_2$ films. *Nature*, **353**(6346): 737-740, https://doi.org/10.1038/353737a0.

Paramasivam I, Jha H, Liu N, Schmuki P. 2012. A review of photocatalysis using self-organized $TiO_2$ nanotubes and other ordered oxide nanostructures. *Small*, **8**(20): 3 073-3 103, https://doi.org/10.1002/smll.201200564.

Park H, Kim K Y, Choi W. 2001. A novel photoelectrochemical method of metal corrosion prevention using a $TiO_2$ solar panel. *Chemical Communications*, (3): 281-282, https://doi.org/10.1039/b008106j.

Park J H, Kim J S, Park J M. 2013. Electrophoretic deposition of nano-ceramics for the photo-generated cathodic corrosion protection of steel substrates. *Surface and Coatings Technology*, **236**: 172-181, https://doi.org/10.1016/j.surfcoat.2013.09.044.

Ren J F, Qian B, Li J Z, Song Z W, Hao L, Shi J S. 2016. Highly efficient polypyrrole sensitized $TiO_2$ nanotube films for photocathodic protection of Q235 carbon steel. *Corrosion Science*, **111**: 596-601, https://doi.org/10.1016/j.corsci.2016.06.001.

Roy P, Berger S, Schmuki P. 2011. $TiO_2$ nanotubes: synthesis and applications. *Angewandte Chemie International Edition*, **50**(13): 2 904-2 939, https://doi.org/10.1002/anie.201001374.

Shao J, Zhang Z D, Wang X T, Zhao X D, Ning X B, Lei J, Li X R, Hou B R. 2018. Synthesis and photocathodic protection properties of nanostructured SnS/$TiO_2$ composites. *Journal of The Electrochemical Society*, **165**(10): H601-H606, https://doi.org/10.1149/2.0281810jes.

Shen G X, Chen Y C, Lin C J. 2005. Corrosion protection of 316 L stainless steel by a $TiO_2$ nanoparticle coating prepared by sol–gel method. *Thin Solid Films*, **489**(1-2): 130-136, https://doi.org/10.1016/j.tsf.2005.05.016.

Subasri R, Deshpande S, Seal S, Shinohara T. 2006. Evaluation of the performance of $TiO_2$-$CeO_2$ bilayer coatings as photoanodes for corrosion protection of copper. *Electrochemical and Solid State Letters*, **9**(1): B1-B4, https://doi.org/10.1149/1.2133723.

Subasri R, Shinohara T. 2003. Investigations on $SnO_2$-$TiO_2$ composite photoelectrodes for corrosion protection. *Electrochemistry Communications*, **5**(10): 897-902, https://doi.org/10.1016/j.elecom.2003.08.016.

Sun M M, Chen Z Y, Bu Y Y, Yu J Q, Hou B R. 2014. Effect of ZnO on the corrosion of zinc, Q235 carbon steel and 304 stainless steel under white light illumination. *Corrosion Science*, **82**: 77-84, https://doi.org/10.1016/j.corsci.2013.12.022.

Sun M M, Chen Z Y, Bu Y Y. 2015. Enhanced photoelectrochemical cathodic protection performance of the $C_3N_4$@$In_2O_3$ nanocomposite with quasi-shell-core structure under visible light. *Journal of Alloys and Compounds*, **618**: 734-741, https://doi.org/10.1016/j.jallcom.2014.08.234.

Sun M M, Chen Z Y, Li J R, Hou J, Xu F L, Xu L K, Zeng R C. 2018a. Enhanced visible light-driven activity of $TiO_2$ nanotube array photoanode co-sensitized by “green”

$AgInS_2$ photosensitizer and $In_2S_3$ buffer layer. *Electrochimica Acta*, **269**: 429-440, https://doi.org/10.1016/j.electacta.2018.03.035.

Sun M M, Chen Z Y, Yu J Q. 2013. Highly efficient visible light induced photoelectrochemical anticorrosion for 304 SS by Ni-doped $TiO_2$. *Electrochimica Acta*, **109**: 13-19, https://doi.org/10.1016/j.electacta.2013.07.121.

Sun M M, Chen Z Y. 2015. Enhanced photoelectrochemical cathodic protection performance of the $In_2O_3/TiO_2$ composite. *Journal of the Electrochemical Society*, **162**(3): C96-C104, https://doi.org/10.1149/2.0381503jes.

Sun W X, Cui S W, Wei N, Chen S G, Liu Y P, Wang D A. 2018b. Hierarchical $WO_3/TiO_2$ nanotube nanocomposites for efficient photocathodic protection of 304 stainless steel under visible light. *Journal of Alloys and Compounds*, **749**: 741-749, https://doi.org/10.1016/j.jallcom.2018.03.371.

Tatsuma T, Saitoh S, Ohko Y, Fujishima A. 2001. $TiO_2$-$WO_3$ photoelectrochemical anticorrosion system with an energy storage ability. *Chemistry of Materials*, **13**(9): 2 838-2 842, https://doi.org/10.1021/cm010024k.

Tong H, Ouyang S X, Bi Y P, Umezawa N, Oshikiri M, Ye J H. 2012. Nano-photocatalytic materials: possibilities and challenges. *Advanced Materials*, **24**(2): 229-251, https://doi.org/10.1002/adma.201102752.

Tsutsumi Y, Nishikata A, Tsuru T. 2006. Monitoring of rusting of stainless steels in marine atmospheres using electrochemical impedance technique. *Journal of the Electrochemical Society*, **153**(7): B278, https://doi.org/10.1149/1.2202110.

Tsutsumi Y, Nishikata A, Tsuru T. 2007. Pitting corrosion mechanism of Type 304 stainless steel under a droplet of chloride solutions. *Corrosion Science*, **49**(3): 1 394-1 407, https://doi.org/10.1016/j.corsci.2006.08.016.

Wang R, Hashimoto K, Fujishima A, Chikuni M, Kojima E, Kitamura A, Shimohigoshi M, Watanabe T. 1998. Photogeneration of highly amphiphilic $TiO_2$ surfaces. *Advanced Materials*, **10**(2): 135-138, https://doi.org/10.1002/(sici)1521-4095(199801)10:2<135::aid-adma135>3.0.co;2-m.

Wang W C, Wang X T, Wang N, Ning X B, Li H, Lu D Z, Liu X J, Zhang Q C, Huang Y L. 2018a. $Bi_2Se_3$ sensitized $TiO_2$ nanotube films for photogenerated cathodic protection of 304 stainless steel under visible light. *Nanoscale Research Letters*, **13**(1): 295, https://doi.org/10.1186/s11671-018-2717-9.

Wang X T, Lei J, Shao Q, Li X R, Ning X B, Shao J, Duan J Z, Hou B R. 2019. Preparation of $ZnWO_4/TiO_2$ composite film and its photocathodic protection for 304 stainless steel under visible light. *Nanotechnology*, **30**(4): 045710. http://doi.org/10.1088/1361-6528/aaef9c.

Wang X T, Ning X B, Shao Q, Ge S S, Fei Z Y, Lei J, Hou B R. 2018b. ZnFeAl-layered double hydroxides/$TiO_2$ composites as photoanodes for photocathodic protection of 304 stainless steel. *Scientific Reports*, **8**(1): 4 116, https://doi.org/10.1038/s41598-018-22572-7.

Wang X T, Wei Q Y, Li J R, Li H, Zhang Q X, Ge S S. 2016a. Preparation of $NiSe_2/TiO_2$ nanocomposite for photocathodic protection of stainless steel. *Materials Letters*, **185**: 443-446, https://doi.org/10.1016/j.matlet.2016.09.052.

Wang X T, Wei Q Y, Zhang L, Sun H F, Li H, Zhang Q X. 2016b. CdTe/$TiO_2$ nanocomposite material for photogenerated cathodic protection of 304 stainless steel. *Materials Science and Engineering*: *B*, **208**: 22-28, https://doi.org/10.1016/j.mseb.2016.02.006.

Wei N, Liu Y, Zhang T T, Liang J, Wang D A. 2016. Hydrogenated $TiO_2$ nanotube arrays with enhanced photoelectrochemical property for photocathodic protection under visible light. *Materials Letters*, **185**: 81-84, https://doi.org/10.1016/j.matlet.2016.08.109.

Xie X, Liu L, Chen R Z, Liu G, Li Y, Wang F H. 2018. Long-term photoelectrochemical cathodic protection by $Co(OH)_2$-modified $TiO_2$ on 304 stainless steel in marine environment. *Journal of the Electrochemical Society*, **165**(4):H3154-H3163,https://doi.org/10.1149/2.0221804jes.

Xie X, Liu L, Chen R Z, Liu G, Li Y, Wang F H. 2019. Design of new al photoanode composite for cathodic protection based on photocatalytic material and sacrificial anode. *Journal of the Electrochemical Society*, **166**(5): H3215-H3222, https://doi.org/10.1149/2.0321905jes.

Xu D W, Yang M K, Liu Y, Zhu R, Lv X D, Zhang C, Liu B. 2020. Fabrication of an innovative designed $TiO_2$ nanosheets/CdSe/polyaniline/graphene quaternary composite and its application as in-situ photocathodic protection coatings on 304SS. *Journal of Alloys and Compounds*, **822**: 153685, https://doi.org/10.1016/j.jallcom.2020.153685.

Xu H M, Liu W, Cao L X, Su G, Duan R J. 2014. Preparation of porous $TiO_2$/ZnO composite film and its photocathodic protection properties for 304 stainless steel. *Applied Surface Science*, **301**: 508-514, https://doi.org/10.1016/j.apsusc.2014.02.114.

Xue J B, Gao J L, Shen Q Q, Li Q, Liu X G, Jia H S, Wu Y C. 2020. Performance of photocatalytic cathodic protection of 20 steel by α-$Fe_2O_3/TiO_2$ system. *Surface and Coatings Technology*, **385**: 125445, https://doi.org/10.1016/j.surfcoat.2020.125445.

Yang H G, Liu G, Qiao S Z, Sun C H, Jin Y G, Smith S C, Zou J, Cheng H M, Lu G Q. 2009. Solvothermal synthesis and photoreactivity of anatase $TiO_2$ nanosheets with dominant {001} facets. *Journal of the American Chemical Society*, **131**(11): 4 078-4 083, https://doi.org/10.1021/ja808790p.

Yang H M, Deng M M, Zeng Q X, Zhang X M, Hu J, Tang Q, Yang H K, Hu C G, Xi Y, Wang Z L. 2020. Polydirectional microvibration energy collection for self-powered multifunctional systems based on hybridized nanogenerators. *ACS Nano*, **14**(3): 3 328-3 336, https://doi.org/10.1021/acsnano.9b08998.

Yang Y Y, Zhang W W, Xu Y, Sun H Q, Wang X M. 2019. $Ag_2S$ decorated $TiO_2$ nanosheets grown on carbon fibers for photoelectrochemical protection of 304 stainless steel. *Applied Surface Science*, **494**: 841-849, https://doi.org/10.1016/j.apsusc.2019.07.234.

Yang Y, Cheng Y F. 2018. One-step facile preparation of ZnO nanorods as high-performance photoanodes for photoelectrochemical cathodic protection. *Electrochimica Acta*, **276**: 311-318, https://doi.org/10.1016/j.electacta.2018.04.206.

Yu S Q, Ling Y H, Wang R G, Zhang J, Qin F, Zhang Z J. 2018. Constructing superhydrophobic $WO_3$@$TiO_2$ nanoflake surface beyond amorphous alloy against electrochemical corrosion on iron steel. *Applied Surface Science*, **436**: 527-535, https://doi.org/10.1016/j.apsusc.2017.11.211.

Yuan J N, Fujisawa R, Tsujikawa S. 1994. Photopotentials of copper coated with $TiO_2$ by sol-gel method. *Zairyo-to-Kankyo*, **43**(8): 433-440, https://doi.org/10.3323/jcorr1991.43.433.

Yuan J N, Tsujikawa S. 1995. Characterization of sol-gel-derived $TiO_2$ coatings and their photoeffects on copper substrates. *Journal of the Electrochemical Society*, **142**(10): 3 444-3 450, https://doi.org/10.1149/1.2050002.

Zhang H M, Liu P R, Wang H J, Yu H, Zhang S Q, Zhu H Y, Peng F, Zhao H J. 2010. Facile formation of branched titanate nanotubes to grow a three-dimensional nanotubular network directly on a solid substrate. *Langmuir*, **26**(3): 1 574-1 578, https://doi.org/10.1021/la9041869.

Zhang J, Hu J, Zhu Y F, Liu Q, Zhang H, Du R G, Lin C J. 2015a. Fabrication of CdTe/ZnS core/shell quantum dots sensitized $TiO_2$ nanotube films for photocathodic protection of stainless steel. *Corrosion Science*, **99**: 118-124, https://doi.org/10.1016/j.corsci.2015.06.029.

Zhang L, Wang X T, Liu F G, Sun H F, Li H, Wei Q Y, Hou B R. 2015b. Photogenerated cathodic protection of 304ss by ZnSe/$TiO_2$ NTs under visible light. *Materials Letters*, **143**: 116-119, https://doi.org/10.1016/j.matlet.2014.12.047.

Zhang T T, Liu Y P, Liang J, Wang D A. 2017a. Enhancement of photoelectrochemical and photocathodic protection properties of $TiO_2$ nanotube arrays by simple surface UV treatment. *Applied Surface Science*, **394**: 440-445, https://doi.org/10.1016/j.apsusc.2016.10.120.

Zhang W W, Guo H L, Sun H Q, Zeng R C. 2017b. Constructing ternary polyaniline-graphene-$TiO_2$ hybrids with enhanced photoelectrochemical performance in photo-generated cathodic protection. *Applied Surface Science*, **410**: 547-556, https://doi.org/10.1016/j.apsusc.2017.03.133.

Zhang Y, Bu Y Y, Yu J Q, Li P. 2013. Highly efficient photoelectrochemical performance of $SrTiO_3$/$TiO_2$ heterojunction nanotube array thin film. *Journal of Nanoparticle Research*, **15**(6): 1 717, https://doi.org/10.1007/s11051-013-1717-z.

Zhou M J, Zeng Z O, Zhong L. 2009. Photogenerated cathode protection properties of nano-sized $TiO_2$/$WO_3$ coating. *Corrosion Science*, **51**(6): 1 386-1 391, https://doi.org/10.1016/j.corsci.2009.03.024.

Zhou M J, Zhang N, Zhang L, Yan J H. 2012. Photocathodic protection properties of $TiO_2$-$V_2O_5$ composite coatings. *Materials and Corrosion-Werkstoffe Und Korrosion*, **64**(11): 996-1 000, https://doi.org/10.1002/maco.201106418.

Zhu Y F, Du R G, Chen W, Qi H Q, Lin C J. 2010. Photocathodic protection properties of three-dimensional titanate nanowire network films prepared by a combined sol-gel and hydrothermal method. *Electrochemistry Communications*, **12**(11): 1 626-1 629, https://doi.org/10.1016/j.elecom.2010.09.011.

Zhu Y F, Liu Y W, Yang Z N. 2019. Highly efficient photo-induced cathodic protection of 403SS by the all-solid-state Z-scheme ZnS-CdS-Ag@$TiO_2$ Nanoheterojunctions. *International Journal of Electrochemical Science*, **14**: 815-825, https://doi.org/10.20964/2019.01.74.

Zhu Y F, Xu L, Hu J, Zhang J, Du R G, Lin C J. 2014. Fabrication of heterostructured $SrTiO_3$/$TiO_2$ nanotube array films and their use in photocathodic protection of stainless steel. *Electrochimica Acta*, **121**: 361-368, https://doi.org/10.1016/j.electacta.2013.12.178.

Zhu Y F, Zhang J, Xu L, Guo Y, Wang X P, Du R G, Lin C J. 2013. Fabrication and photoelectrochemical properties of ZnS/Au/$TiO_2$ nanotube array films. *Physical Chemistry Chemical Physics*, **15**(11): 4 041-4 048, https://doi.org/10.1039/c3cp43572e.

Zuo J, Wu H, Chen A J, Zhu J Q, Ye M D, Ma J D, Qi Z B. 2018. Shape-dependent photogenerated cathodic protection by hierarchically nanostructured $TiO_2$ films. *Applied Surface Science*, **462**: 142-148, https://doi.org/10.1016/j.apsusc.2018.07.143.